DOKUZ EYLÜL UNIVERSITY

GRADUATE SCHOOL OF NATURAL AND APPLIED SCIENCES

PRODUCTION OF ELECTRODEPOSITED Ni MATRIX NANOCOMPOSITE COATINGS

by

Sıdıka YILDIRIM

September, 2016

İZMİR

PRODUCTION OF ELECTRODEPOSITED Ni MATRIX NANOCOMPOSITE COATINGS

A Thesis Submitted to the
Graduate School of Natural and Applied Sciences of Dokuz Eylül University
In Partial Fulfillment of the Requirements for the Degree of Master of Science in Metallurgical and Materials Engineering

by
Sıdıka YILDIRIM

September, 2016
İZMİR

M.Sc THESIS EXAMINATION RESULT FORM

We have read the thesis entitled **"PRODUCTION OF ELECTRODEPOSITION Ni MATRIX NANOCOMPOSITE COATINGS"** completed by **SIDIKA YILDIRIM** under supervision of **ASST. PROF. DR. IŞIL BİRLİK** and we certify that in our opinion it is fully adequate, in scope and in quality, as a thesis for the degree of Master of Science .

Asst. Prof. Dr. Işıl BİRLİK

Supervisor

Asst. Prof. Dr. Funda AK AZEM

Jury Member

Assoc. Prof. Dr. Osman CULHA

Jury Member

Prof.Dr. Ayşe OKUR

Director

Graduate School of Natural and Applied Sciences

ACKNOWLEDGMENTS

Firstly, I would like to express to my deep and sincere gratitude to my advisor Assist. Prof. Dr. Işıl BİRLİK and co-advisor Assist. Prof. Dr. N. Funda AK AZEM for their excellent guidance, patient supervision and continuous support thought the preparation of this study.

I warmly express my special thanks to my co-worker, Onur BARDAKÇIOĞLU for his support, help, patience and friendship. I wish to extend my sincere thanks to Serhan KÖKTAŞ, Kadir Cihan TEKİN, Onur ERTUĞRUL, Çağrı KILINÇ, Haydar KAHRAMAN, Ramazan DALMIŞ, Dalyan ÖZKAN, Oylum ÇOLPANKAN, Tuncay DİKİCİ and Orkut SANCAKOĞLU, for their helps during my experiments. In addition, I would like to thank Tülay KOÇ DELİCE, Bensu BAKIN, Utku TİRİÇ, Elif ELDEN and Mehmet Bulut ÖZYİĞİT for their valuable friendships and supports.

The present research was also supported by The Scientific and Technological Research Council of Turkey (TÜBİTAK) with project code 113R023 named as "Production, investigation and industrial utilization of nanocomposite coatings as photoanode applications for cathodic protection systems".

Finally, I would like to express my deep and sincere thanks to my family who always believed in me. I especially thank to Serdar GÜLTEKİN for his never-ending support, understanding and encouragement. This thesis work was easier with his presence in my life.

Sıdıka YILDIRIM

PRODUCTION OF ELECTRODEPOSITED Ni MATRIX NANOCOMPOSITE COATINGS

ABSTRACT

The present thesis involves deposition of Ni matrix nanocomposite coatings by electrodeposition method and preparation of titanium dioxide, zinc oxide and silica nanoparticles by sol-gel technique.

First of all, nanosized titanium dioxide, zinc oxide and silica particles were synthesized via sol-gel technique using titanium tetraisopropoxide, Zinc acetate dihydrate and tetraethyl orthosilicate as the precursors, respectively. Structural characterization and particle size distribution measurements of sol-gel synthesized nanoparticles were performed with X-ray difractometer (XRD) and particle size analyzer, respectively. Obtained results indicate that all nanoparticles were synthesized homogeneously and their particle sizes are below 100 nm.

Afterwards, pure Ni and Ni matrix nanocomposite coatings were prepared by electrodeposition method. The effect of preparation parameters, such as current density, nanoparticles size and concentration on the formation of nanocomposite coatings has been analyzed. Crystalline structure of nanocomposite coatings was analyzed using XRD. Also, surface morphology and elemental composition of the coatings were investigated by using Scanning Electron Microscope (SEM) coupled with Energy Dispersive Spectrometer (EDS). Corrosion properties of the coatings were studied by potentiodynamic polarization technique in NaCl solution. Compared to electrodeposited pure nickel coating, the produced nanocomposites exhibit improved corrosion resistance.

Keywords: Nanoparticle, sol-gel, nickel coating, nanocomposite, electrodeposition, corrosion

ELEKTROÇÖKTÜRME YÖNTEMİ İLE Ni MATRİS NANOKOMPOZİT KAPLAMALARIN ÜRETİMİ

ÖZ

Sunulan bu tez elektroçöktürme yöntemiyle Ni matrix nanokompozit kaplamaların çöktürülmesini ve titanyum dioksit, çinko oksit ve silika nanopartiküllerinin sol-jel yöntemi ile hazırlanmasını içermektedir.

İlk olarak, nanoboyutlu titanyum dioksit, çinko oksit ve silika partikülleri sırasıyla titanyum tetra izopropoksit, çinko asetat dihidrat ve tetra etil orto silikat başlangıç kimyasalları kullanılarak sol-jel yöntemiyle sentezlenmiştir. Sol-jel yöntemiyle sentezlenen nanopartiküllerin yapısal karakterizasyonları ve partikül boyut dağılımı ölçümleri sırasıyla X ışını difraktometresi (XRD) ve partikül boyut analizi cihazlarıyla gerçekleştirilmiştir. Elde edilen sonuçlar bütün nanopartiküllerin homojen olarak sentezlendiğini ve partikül boyutların 100 nm'nin altında olduğunu göstermektedir.

Daha sonra, saf nikel ve Ni matrisli nanokompozit kaplamalar elektroçöktürme yöntemiyle hazırlanmıştır. Akım yoğunluğu, nanopartikül boyutu ve konsantrasyonu gibi hazırlama parametrelerinin nanokompozit kaplamanın oluşumuna etkisi incelenmiştir. Üretilen nanopartiküllerin ve oluşturulan nanokompozit kaplamaların kristal yapıları XRD cihazıyla analiz edilmiştir. Ayrıca kaplamalarım yüzey morfolojilerini görüntülemek ve kaplama yüzeylerini elementel olarak analiz etmek amacıyla sırasıyla SEM ve EDS cihazı kullanılmıştır. Oluşturulan kaplamaların korozyon özellikleri NaCl çözeltisi kullanılarak potansiyodinamik polarizasyon tekniği ile belirlenmiştir. Üretilen nanokompozit kaplamaların elektroçöktürülmüş saf nikel ile kıyaslandığında daha yüksek korozyon dayanımına sahip olduğu gözlenmektedir.

Anahtar kelimeler: Nanopartikül, sol-jel, nikel kaplama, nanokompozit, elektroçöktürme, korozyon

CONTENTS

Page

THESIS EXAMINATION RESULT FORM ii
ACKNOWLEDGMENTS iii
ABSTRACT iv
ÖZ v
LIST OF FIGURES ix
LIST OF TABLES xiii

CHAPTER ONE - INTRODUCTION 1

CHAPTER TWO - NANOTECHNOLOGY AND NANOMATERIALS 3

2.1 Introduction 3
2.2 Production Techniques of Nanomaterials 4
2.2.1 Inert-gas Condensation 5
2.2.2 Inert-gas Expansion 6
2.2.3 Sonochemical Processing 7
2.2.4 Sol-gel Process 7
2.2.5 Molecular Self-assembly 8
2.2.6 Foil Beating 9
2.2.7 Electrodeposition 9
2.2.8 Physical Vapor Deposition (PVD) 9
2.2.9 Chemical Vapor Deposition (CVD) 10
2.3 Sol-Gel Process 11
2.3.1 The Chemistry of Precursors Solution 13
2.3.2 Hydrolysis and Condensation Reaction 14
2.3.3 Gelation 15
2.3.4 Drying and Sintering 16

CHAPTER THREE - NICKEL AND NICKEL MATRIX NANOCOMPOSITE COATINGS 17

3.1 Nickel Coating 17
3.2 Types of Electrolytes for Nickel Coating Process 19
3.2.1 Watts Nickel Bath 19
3.2.2 Sulphamate Nickel Bath 22
3.2.3 Other Electrolyte Types for Nickel Coating Process 22
3.3 Nanocomposite Coating 23
3.3.1 Ceramic Matrix Nanocomposites (CMNC) 26
3.3.2 Metal Matrix Nanocomposites (MMNC) 26
3.3.3 Polymer Matrix Nanocomposites (PMNC) 27
3.4 Nickel Matrix Nanocomposite Coatings 27
3.5 Production of Nickel Matrix Nanocomposite Coatings 29
3.5.1 Electrodeposition Method 30

CHAPTER FOUR - EXPERIMENTAL STUDIES 35

4.1 Production of Nanoparticles 35
4.1.1 Production of TiO_2 Nanoparticles 35
4.1.2 Production of ZnO Nanoparticles 37
4.1.3 Production of SiO_2 Nanoparticles 38
4.2 Preparation of the Substrate 39
4.3 Production of Electrodeposited Pure Nickel and Nickel Matrix Nanocomposite Coatings 39
4.4 Characterization of the Nanoparticles and Nanocomposite Coatings 42
4.4.1 X-ray Diffraction (XRD) 42
4.4.2 Particle Size Analyser 43
4.4.3 Scanning Electron Microscopy (SEM) 43
4.4.4 Electrochemical Method 44

CHAPTER FIVE - RESULTS AND DISCUSSION 45

5.1 Sol-Gel Synthesized Nanoparticles..... 45

5.1.1 Characterization of TiO_2 Nanoparticles 45

5.2 Characterization of ZnO Nanoparticles 47

5.3 Characterization of SiO_2 Nanoparticles 50

5.4 Characterization of Electrodeposited Pure Nickel and Nickel Matrix Nanocomposite Coatings 52

5.4.1 Characterization of Electrodeposited Ni-TiO_2 Nanocomposite Coatings 53

5.4.2 Characterization of Electrodeposited Ni-ZnO Nanocomposite Coatings 56

5.4.3 Characterization of Electrodeposited Ni-SiO_2 Nanocomposite Coatings 58

5.5 Corrosion Behavior of Electrodeposited Pure Nickel and Nickel Matrix Nanocomposite Coatings 61

CHAPTER SIX - CONCLUSION 67

REFERENCES 69

LIST OF FIGURES

Page

Figure 2.1 Typical synthetic methods for nanoparticles. 5
Figure 2.2 Schematic of the inert gas condensation setup. 6
Figure 2.3 Cluster formation by vapor phase expansion from an oven source. 6
Figure 2.4 Sonochemical processing. 7
Figure 2.5 Self-assembly of nanoclusters. The enclosed droplet can be spherical or cylindrical. Reaction within it generates a nanoparticle or nanorod. ... 8
Figure 2.6 Beating of gold leaf 9
Figure 2.7 Physical vapor deposition (PVD). Material, evaporated by heating, by ion bombardment, or by laser ablation, is deposited on a substrate target. The deposited layer can be of nano thickness. 10
Figure 2.8 Various steps in the sol-gel process to control the final morphology of the product. 13
Figure 3.1 Scheme of the different types of nanocomposites. (a) 0D, formed by nanoparticles. (b) 1D, formed by nanotubes. (c) 2D, formed by nanolayers. The matrix is represented by a gray background 25
Figure 3.2 Schematic representation of differentdeposition possibilities 31
Figure 3.3 Simple electrodeposition system. 32
Figure 3.4 Electrical double layer 34
Figure 4.1 Schematic illustration of sol TiO_2-A preparation 36
Figure 4.2 Schematic illustration of sol TiO_2-B preparation. 36
Figure 4.3 Schematic illustration of ZnO nanoparticles preparation by sol-gel technique 37
Figure 4.4 Schematic illustration of SiO_2 nanoparticles preparation by sol-gel technique 38
Figure 4.5 Experimental setup 40
Figure 4.6 Diffraction of x -rays by planes of atoms (A -A ' and B -B ') 42
Figure 5.1 X-ray θ-2θ scans of TiO_2-A and TiO_2-B nanoparticles. 46
Figure 5.2 Distribution chart of particle sizes of (a) TiO_2-A (without gelling agent), (b) TiO_2-B (with gelling agent). 47
Figure 5.3 X-ray θ-2θ scans of ZnO nanoparticles 48

Figure 5.4 Particle size distribution chart of ZnO nanoparticles were synthesized at 0.2 M and pH: 7, 9, 11, 12 49
Figure 5.5 Particle size distribution chart of ZnO nanoparticles were synthesized at 0.1 M and pH: 7, 9, 11, 12 49
Figure 5.6 Particle size distribution chart of ZnO nanoparticles were synthesized at 0.05 M and pH: 7, 9, 11, 12 49
Figure 5.7 Particle size distribution chart of ZnO nanoparticles were synthesized at 0.05 M, pH: 11 and waiting time: 1 day 50
Figure 5.8 XRD results of SiO_2 nanoparticles 51
Figure 5.9 Particle size distribution chart of SiO_2 nanoparticles were synthesized using 0.09, 0045 and 0.0225 molarities 52
Figure 5.10 X-ray θ-2θ scans of Ni coatings at 3, 5 and 7 A dm^{-2} 52
Figure 5.11 X-ray θ-2θ scans of Ni-TiO_2 nanocomposite coatings with TiO_2 nanoparticles (a) 80 nm sized and 1 g/l concentration, (b) 50 nm sized and 1 g/l concentration and (c) 50 nm sized and 3 g/l concentration electrodeposited at 3, 5 and 7 A dm^{-2} current densities. 53
Figure 5.12 Surface morphologies of (a) pure nickel and Ni-TiO_2 nanocomposite coatings with TiO_2 nanoparticles (b) 80 nm sized and 1 g/l concentration, (c) 50 nm sized and 1 g/l concentration and (d) 50 nm sized and 3 g/l concentration electrodeposited at 3, 5 and 7 A dm^{-2} current densities. 55
Figure 5.13 Mapping images of Ni-TiO_2 nanocomposite coatings with 50 nm sized and 3 g/l concentration TiO_2 nanoparticles 56
Figure 5.14 X-ray θ-2θ scans of Ni-ZnO nanocomposite coatings with ZnO nanoparticles (a) 80 nm sized and 1 g/l concentration, (b) 50 nm sized and 1 g/l concentration electrodeposited at 3, 5 and 7 A dm^{-2} current densities. 56
Figure 5.15 Surface morphologies of (a) pure nickel and Ni-ZnO nanocomposite coatings with ZnO nanoparticles (b) 80 nm sized and 1 g/l concentration, (c) 50 nm sized and 1 g/l concentration electrodeposited at 3, 5 and 7 A dm^{-2} current densities. 57
Figure 5.16 Mapping images of Ni-ZnO nanocomposite coatings with 50 nm sized and 1 g/l concentration ZnO nanoparticles 58

Figure 5.17 X-ray θ-2θ scans of Ni-SiO_2 nanocomposite coatings with SiO_2 nanoparticles (a) 80 nm sized and 1 g/l concentration, (b) 50 nm sized and 1 g/l concentration and (c) 50 nm sized and 3 g/l concentration electrodeposited at 3, 5 and 7 A dm^{-2} current densities..... 59

Figure 5.18 Surface morphologies of (a) pure nickel and Ni-SiO_2 nanocomposite coatings with SiO_2 nanoparticles (b) 80 nm sized and 1 g/l concentration, (c) 50 nm sized and 1 g/l concentration and (d) 50 nm sized and 3 g/l concentration electrodeposited at 3, 5 and 7 A dm^{-2} current densities. 60

Figure 5.19 Mapping images of Ni-SiO_2 nanocomposite coatings with 50 nm sized and 3 g/l concentration SiO_2 nanoparticles 61

Figure 5.20 Comparative potentiodynamic diagrams of pure nickel and Ni-TiO_2 nanocomposite coatings with TiO_2 nanoparticles (a) 80 nm sized and 1 g/l concentration, (b) 50 nm sized and 1 g/l concentration and (c) 50 nm sized and 3 g/l concentration electrodeposited at 3, 5 and 7 A dm^{-2} current densities. 63

Figure 5.21 Comparative potentiodynamic diagrams of pure nickel and Ni-ZnO nanocomposite coatings with ZnO nanoparticles (a) 80 nm sized and 1 g/l concentration, (b) 50 nm sized and 1 g/l concentration electrodeposited at 3, 5 and 7 A dm^{-2} current densities..... 64

Figure 5.22 Comparative potentiodynamic diagrams of pure nickel and Ni-SiO_2 nanocomposite coatings with SiO_2 nanoparticles (a) 80 nm sized and 1 g/l concentration, (b) 50 nm sized and 1 g/l concentration and (c) 50 nm sized and 3 g/l concentration electrodeposited at 3, 5 and 7 A dm^{-2} current densities..... 65

LIST OF TABLES

Page

Table 2.1 Nanomaterials are categorised according to their dimensions. 3
Table 3.1 Typical formula and operating conditions for Watts nickel electroplating solutions. 20
Table 3.2 Typical composition and operating conditions for nickel sulphamate electroplating solutions 22
Table 3.3 Different types of nanocomposites. 26
Table 4.1 Etching solution 39
Table 4.2 Composition of the electrodeposition bath 40
Table 4.3 Overwiew of the electrodeposition parameters of Nickel and Ni matrix nanocomposite coatings 41
Table 4.4 Nomenclature of the coatings according to the deposition parameters. 41
Table 5.1 Particle size values of TiO_2 nanoparticles 47
Table 5.2 Particle size value of ZnO nanoparticles 50
Table 5.3 Particle size values of SiO_2 nanoparticles were synthesized using different molarities 52
Table 5.4 Corrosion characteristics Ni-TiO_2 nanocomposite coatings 63
Table 5.5 Corrosion characteristics Ni-ZnO nanocomposite coatings 64
Table 5.6 Corrosion characteristics Ni-SiO_2 nanocomposite coatings 66

CHAPTER ONE
INTRODUCTION

Nanotechnology is the science that deals with matter at the scale of 1 billionth of a meter (i.e., 10^{-9} m = 1 nm), and is also the study of manipulating matter at the atomic and molecular scale (Horikoshi & Serpone, 2013). Nanomaterials, defined as particles ranging from 1 to 100 nm diameter, have become widely utilized because of their unique physicochemical properties (Macwan, Dave & Chaturvedi, 2011). There are numerous methods for synthesizing nanomaterials with various characteristics (Qiao, Liu & Lu, 2011).

The sol-gel method as recently developed as a general and powerful approach for preparing inorganic materials. This method for synthesis of inorganic materials has a number of advantages over more conventional synthetic procedures. For example, high-purity materials can be synthesized at low temperatures. In addition, homogeneous multi component systems can be obtained by mixing precursor solutions, which allows for easy chemical doping of the materials prepared (Sangchay, Sikong & Kooptarnond, 2012).

The recent trend in surface engineering researches was predominantly focused on the improvement of steels surfaces which were widely utilized in various industries as a required commercial material (Rostami, Fahami, Nasiri-Tabrizi, Ebrahimi-Kahrizsangi & Saatchi, 2013). Applying a coating on the surface is a method to improve the surface properties. Several techniques have been applied to produce protective coatings, such as electrodeposition, plasma thermal spray and physical vapor deposition methods (Baghery, Farzam, Mousavi & Hosseini, 2010).

Nickel is one of the most important metals applied by electro-deposition (Sadiku-Agboola, Sadiku, Ojo, Akanji & Biotidara, 2011). However, the nickel-deposited surface shows low surface mechanical properties and to improve this electrodeposition of Ni with non-metal was investigated regularly. The electro-co-deposition of Ni with second phase hard inert particles such asmetal oxides, metal

carbides, nitrides, borides (TiO_2, ZrO_2, SiO_2, Al_2O_3, Cr_2O_3, SiC, WC, TiC, Cr_3C_2, Si_3N_4, BN, and ZrB), carbon nanotube (CNTs), and diamond are generally used in composite coating to improve properties such as hardness, wear resistance, and corrosion resistance (Parida, Chaira, Chopkar & Basu, 2011).

The goal of the study was to produce Ni matrix nanocomposite coatings on steel substrates for improving corrosion properties of the coatings.

The structure of the thesis consists of five different parts in addition to this chapter which are summarized below:

Chapter 2 is a literature review, including nanomaterials and production techniques. Sol-gel which is most common technique was reviewed in detail.

Chapter 3 is a literature review, including Ni coating and different types of Ni coating baths, nanocomposite coatings, Ni matrix nanocomposite coatings production techniques. Electrodeposition as a production technique was reviewed in detail.

Chapter 4 is on the experimental work conducted, including production of nanoparticles, preparation of the substrate, production of electrodeposited pure Ni and Ni matrix nanocomposite coatings, characterization techniques and electrochemical measurements.

Chapter 5 presents results and discussions, including XRD and particle size measurements of nanoparticles and XRD, SEM, electrochemical measurements results of pure Ni and Ni matrix nanocomposite coatings.

Chapter 6 reviews the main conclusions of the study.

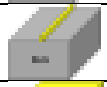
CHAPTER TWO
NANOTECHNOLOGY AND NANOMATERIALS

2.1 Introduction

Nanotechnology is the design, characterization, production and application of structures, devices and systems by controlling shape and size at nanometer scale. The nanometer scale is conventionally defined as 1 to 100 nm. One nanometer is one billionth of a meter (10^{-9} m). The size range is normally set to a minimum of 1 nm to avoid single atoms or very small groups of atoms being designated as nano-objects. Therefore, nanoscience and nanotechnologies deal with clusters of atoms of 1 nm in at least one dimension (Fiiipponi & Sutherland, 2012).

A nanomaterial is an object that has at least one dimension in the nanometre scale (approximately 1 to 100 nm). Nanomaterials are categorised according to their dimensions as shown in Table 2.1(Fiiipponi & Sutherland, 2012) .

Table 2.1 Nanomaterials are categorised according to their dimensions (Fiiipponi & Sutherland, 2012).

	Nanomaterial dimension	Example
	All three dimensions < 100 nm	Nanoparticles, quantum dots, nanoshells, nanorings, microcapsules
	Two dimensions < 100 nm	Nanotubes, fibres, nanowires
	One dimension < 100 nm	Thin films, layers and coatings

The most fundamental component in the production of a nanostructure is a nanoparticle. This nanoparticles are far smaller than the world of everyday objects that are described by Newton ' s laws of motion, but bigger than an atom or a simple molecule that are governed by quantum mechanics (Horikoshi & Serpone, 2013). Despite of the fact that there is no a unique definition to identify the nanoparticles, they are usually defined as particles ranging from 1 to 100 nm diameter. The physical properties of the materials start to change below that size. Nanoscaled particles show different and improved properties when compared with their larger size (distribution,

morphology, phase, etc.) (Macwan et al., 2011; Willems, 2005). The physical properties of the particles can be leaded by changing their size from microscale to nano. One of the most effective factors is increasing in the ratio of surface area to volume, the other is the size of the particle moving into the region where quantum effects predominate. Thanks to this large surface area, a lot of interactions occur between the intermixed materials in nanocomposite. This interactions leading to special properties such as increased strength and/or increased chemical/heat resistance (Holister, Weener, Vas & Harper, 2003). One of the most salient changing properties with decreasing size is the optic properties. For example, a 20-nm gold nanoparticle is wine red color, silver nanoparticle is yellowish gray and platinum and palladium nanoparticles are black.

The wide range of material oxide ceramics, such as titanium, zinc, aluminum and iron oxide, metals, silicates (silicates or silicon oxides) and non-oxide ceramics can be produce in nanoscale. Even though nanoparticles of other materials exist, e.g. those based on polymer materials or compound semiconductors, the former categories count for the most part of current applications (Willems, 2005; Holister et al., 2003).

2.2 Production Techniques of Nanomaterials

There are various methods to synthesize nanomaterials with numerous characteristics such as, different size and shape, composition and surface structure, charge, and functionality (Qiao et al., 2011).

Two main approaches which are top down and bottom up are used in literature to synthesize nanomaterials and fabricate nanostructures. Bottom-up approach starts with relatively smaller component (up to atomic level) with further self-assembly process resulting to formation of nanostructure. There are different methods in this approach such as quantum dot formation during epitaxial growth and formation of nanoparticles from colloidal dispersion. On the other hand, researchers choose relatively larger initial structures in top-down approach. These structures can be

externally-controlled in the processing of nanostructures by etching through the mask, ball milling, and application of severe plastic deformation (Baron, Szewieczek & Nowosielski, 2007)

Production techniques of nanomaterials can also be classified according to their dimensions. Various preparation techniques of 0-D, 1-D and 2-D nanomaterials are summarized in Figure 2.1 (Schodek, Ferreira & Ashby, 2009).

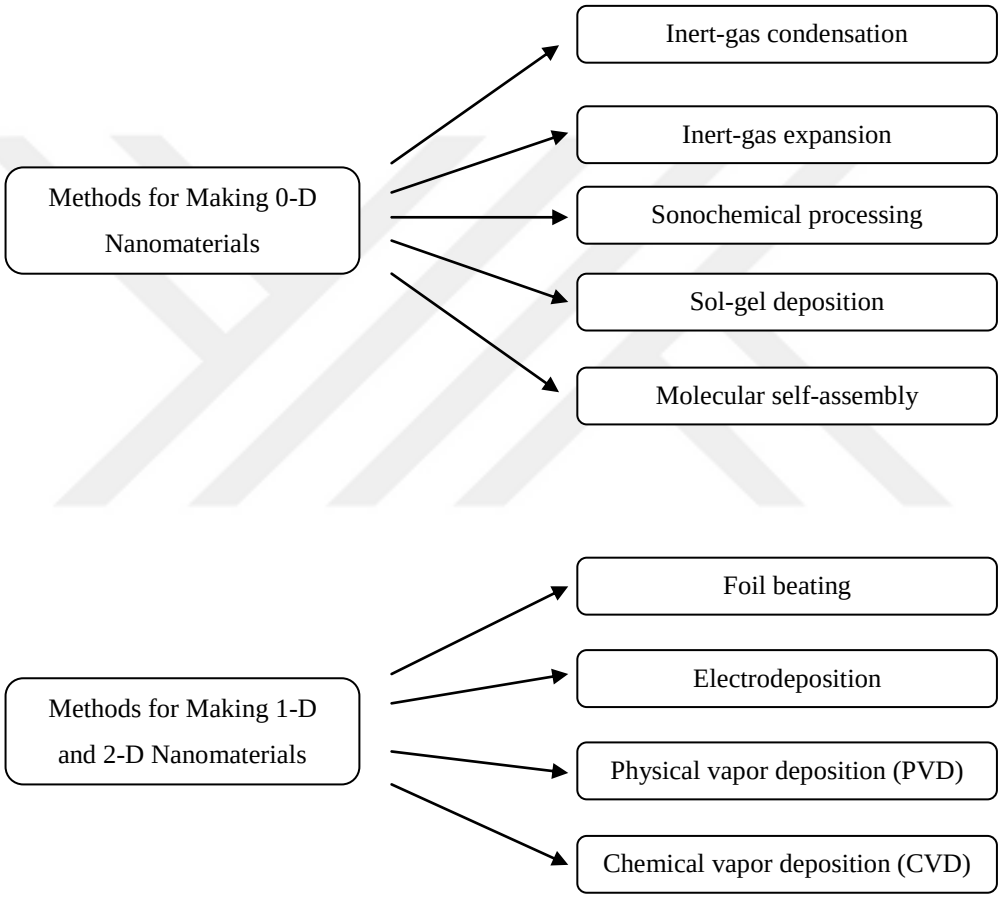


Figure 2.1 Typical synthetic methods for nanoparticles (Schodek et al., 2009).

2.2.1 Inert-gas Condensation

The general perception was that considerable control could be exercised on the particle size, shape, and extent of aggregation if gas condensation processes could be

carried out either in a low-pressure environment, or the nanoparticles were quenched rapidly as soon as they were formed. Accordingly, Granquist and Buhrmann initially synthesized metal nanoparticles by the inert gas condensation (IGC) process. The nanoparticles, some of them with a mean size of 10 nm and smaller were formed when metal atoms effusing from a thermal source rapidly lost their energy by collisions with gas atoms. Figure 2.2 is a schematic of the setup used by the authors to produce metal nanoparticles (Gogotsi, 2006).

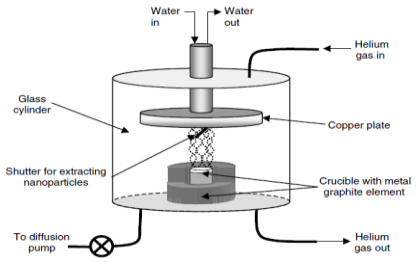


Figure 2.2 Schematic of the inert gas condensation setup (Gogotsi, 2006).

2.2.2 Inert-gas Expansion

In inert-gas or free-jet expansion, evaporated atoms are carried by a high-pressure helium gas stream that is expanded from a nozzle into a low-pressure chamber at supersonic velocities (Figure 2.3). The adiabatic expansion of the gas leads to sudden cooling, causing the evaporated atoms to form clusters a few nanometers in diameter. As in the case of inert-gas condensation, the agglomeration of nanoparticles is a problem, requiring careful control of evaporation rate and inert gas flow; it is these that determine the particle size and distribution (Schodek et al., 2009).

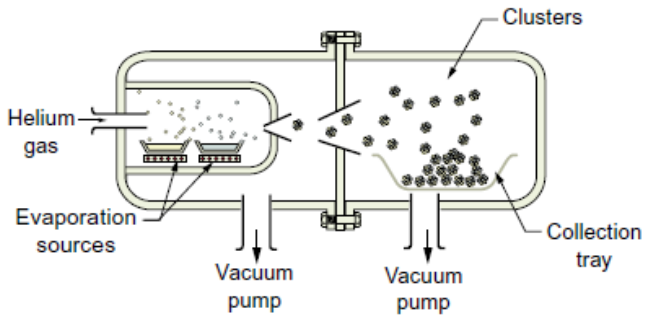


Figure 2.1 Cluster formation by vapor phase expansion from an oven source (Schodek et al., 2009).

2.2.3 Sonochemical Processing

In sonochemical processing, ultrasound is used to nucleate a chemical reaction. A magnetostrictive or piezoelectric transducer (or "horn") is used to generate ultrasonic waves with a wavelength of 1–10,000 microns in a liquid-filled reaction vessel (Figure 2.4). The reaction comes about because of cavitation. The tensile part of the wave is intense enough to pull the liquid apart and form a tiny cavity. The compression part of the wave then compresses it, but before it does, some reactants vaporize inside it. The next tensile wave re-expands the bubble, which oscillates in volume at the frequency of the sound waves, pumping it up as more vapors enters during the expansion part of the cycle. When the bubble reaches a critical size, it collapses. The collapse is adiabatic because the very fast collapse rate leaves no time for heat flow, generating a tiny, localized hot spot. The temperatures are very high (as high as 5000°C, near that of the surface temperature of the sun) and so too are the pressures (around 2000 atmospheres, roughly those at the bottom of deep oceans), triggering reactions that create a nanoparticle within the spot. The size of the spot determines the size of the resulting particles(Schodek et al., 2009).

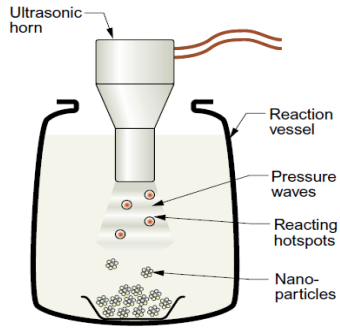


Figure 2.2 Sonochemical processing (Schodek et al., 2009).

2.2.4 Sol-gel Process

Sol-gel method is a long established industrial process for generating colloidal nanoparticles from liquid phase. It has been further developed in the last years for the production of advanced nanomaterials and coatings (Charitidis, Georgiou, Koklioti, Trompeta & Markakis, 2014). Ultrafine particles, nano thickness films, and nano

porous membranes can be made by sol-gel processing (Schodek et al., 2009). This method will be interviewed in detail on section 2.3.

2.2.5 Molecular self-assembly

Molecular self-assembly methods rely on the self-organization of organic molecules. The idea is to create the conditions under which atoms or molecules will self-assemble into useful structures, driven by the minimization of their energy. The great advantage of self-assembly is that the system converges to a specific configuration without the need for further control. Typically, the aggregates formed by self-assembly tend to be bonded by relatively weak bonds with binding energies only a few times larger than kT, the thermal energy per atom. The self-assembling molecules form micelles. Micelles are aggregates of amphiphilic molecules-molecules with one end that is soluble in water and the other end that rejects it. These aggregates form spontaneously at a size that depends on the concentration of the amphiphilic molecules in solution. The center of the micelles acts as a chamber for chemical reactions and thus dictates the size of the nanoparticles created (Figure 2.5) (Schodek et al., 2009).

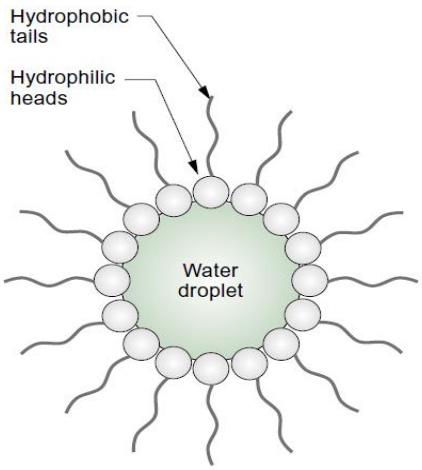


Figure 2.3 Self-assembly of nanoclusters. The enclosed droplet can be spherical or cylindrical. Reaction within it generates a nanoparticle or nanorod (Schodek et al., 2009).

2.2.6 Foil Beating

Gilding is the art of applying gold leaf to a surface. It was known to the ancients, is mentioned in the Old Testament, and was described by Herodotus in 420 BC. Gold is an expensive material; there are obvious incentives to use as little of it as possible. Gold leaf is made by beating the metal to a uniformly thin foil, roughly 100 nm thick (Figure 2.6). It is applied by smoothing it onto the adhesive coated surface of the object to be gilded. There are less labor-intensive ways to make thin films. Electrodeposition is one, and it is one able to create nanoscale structures as well (Schodek et al., 2009)

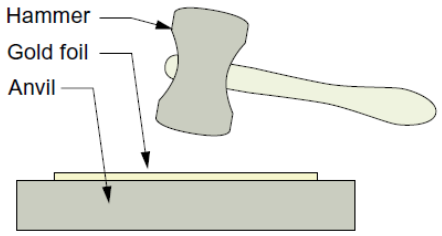


Figure 2.4 Beating of gold leaf (Schodek et al., 2009)

2.2.7 Electrodeposition

Electrodeposition is a producing of a metal coating process onto a substrate. In this process the metal ions in the electrolyte electrochemically reduced. These metal ions in electrolyte solution are transported to the substrate surface leading metal coating. The deposition process can be either cathodic or anodic reaction depending on the work piece to be coated (cathode or anode). Different type of nanostructures such as nanocrystallines, nanocomposites, amorphous film or layered materials can be formed by controlling the electrolysis parameters (Al-Bat'hi, 2015; Kalska-Szostko, 2012). This method will be explained in detail on section 3.5.1.

2.2.8 Physical Vapor Deposition (PVD)

In PVD plating, a thin layer of a material, usually a metal, is deposited from a vapor onto the object to be coated (Figure 2.7). The vapor is created in a vacuum

chamber by direct heating or electron beam heating of the metal, from which it condenses onto the cold substrate, much like steam from a hot bath condensing on a bathroom mirror. In PVD plating there is no potential difference between bath and work piece. In PVD ion plating the vapor is ionized and accelerated by an electric field (the work piece is the cathode, and the metalizing source material is the anode). In PVD sputtering, argon ions are accelerated by the electric field onto a metal target, ejecting ions onto the component surface. By introducing a reactive gas, compounds can be formed. (Sputtering titanium in an atmosphere of nitrogen, for instance, gives a coating of hard TiN.)

Almost any metal or compound that doesn't decompose chemically can be sputtered, making this a very flexible (though expensive) process. Targets can be changed during the process, allowing multilayers to be built up. These multilayers can have remarkable mechanical and electronic properties (Schodek et al., 2009).

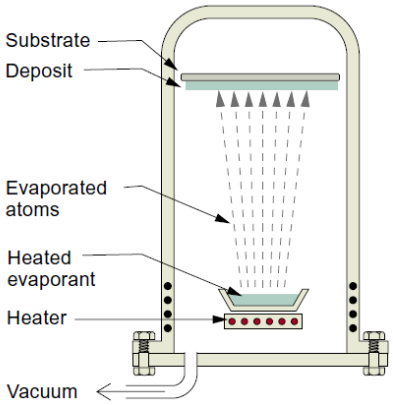


Figure 2.5 Physical vapor deposition (PVD). Material, evaporated by heating, by ion bombardment, or by laser ablation, is deposited on a substrate target. The deposited layer can be of nano thickness (Schodek et al., 2009).

2.2.9 Chemical Vapor Deposition (CVD)

In this approach, vapor phase precursors are brought into a hot-wall reactor under conditions that favor nucleation of particles in the vapor phase rather than deposition of a film on the wall. It is called chemical vapor synthesis or chemical vapor condensation in analogy to the chemical vapor deposition (CVD) processes used to

deposit thin solid films on surfaces. This method has tremendous flexibility in producing a wide range of materials and can take advantage of the huge database of precursor chemistries that have been developed for CVD processes. The precursors can be solid, liquid or gas at ambient conditions, but are delivered to the reactor as a vapor (froma bubbler or sublimation source, as necessary) (Swihart, 2003).

2.3 Sol-Gel Process

Sol-gel techniques have recently held remarkable attention in nanoscience due to its ability to obtain nano structures with chemistry at low temperature and pressure. It is a long-established industrial process for the generation of colloidal nanoparticles from liquid phase that has been further developed in last years for the production of advanced nanomaterials and coatings (Figure 2.8). Furthermore, the sol-gel technique makes it possible to produce material with no toxicity high purity constant composition and reproducibility to be obtained. Also, they are allowed to use in material in contact with food and in pharmaceutical applications. Moreover, controlled structures such as spheres, cylinders, planar two-layered can be obtained with this method when template agents are used (Moncada, Quijada & Retuert, 2007).

The sol-gel process is a synthesis route consisting in the preparation of a sol and successive gelation and solvent removal. It is a chemical method which is based on hydrolysis or condensation reactions (Branda, 2011; Charitidis et al., 2014)

Sol-gel chemistry is a catch all term for the reaction of an organometallic compound, usually an alkoxide or chloride, under aqueous conditions to form a solid product. Many different kind of materials including a dense glass monolith, a high surface area molecular filter, an aerogel, a metal oxide or nitride coating or nanoparticle (Collins, 2012). Ebelmen demonstrated the formation of the first metal alkoxide from $SiCl_4$ in 1844 (Ebelmen, 1846). It was discovered shortly thereafter that exposure to atmospheric moisture formed a gel. A century later Geffcken modified the chemistry towards the production of oxide films (Geffcken, 1939) and

the Schott glass company utilized the gelation of alkoxides to make glass in the 1930s (Hurd, 1938). In the light of these developments, industry has showed big progress to design precursor chemistry in the preparation of ceramics and glasses in sol-gel method at room temperatures (Levene & Thomas, 1979; Collins, 2012).

Sol-gel method has many advantages as compared to other conventional methods. These inherent advantages of the sol-gel process could be listed as follows:

- Better homogeneity and purity from raw materials
- Lower temperature of preparation
- Good mixing for multi-component systems
- Effective control of particle size, shape, and properties
- Better products from the special properties of the gel
- The creation of special products such as films
- The possibility of designing the material structure and property through the proper selection of sol-gel precursor (Tseng, Lin, Chen & Chu, 2010).

Basically, sol-gel synthesis is carried out in a liquid medium. This process involves the evolution of inorganic networks through the formation of a colloidal suspension which is called sol and gelation of the sol to form a network in a continuous liquid phase which is denoted as gel (Qiao et al., 2011). In general, the sol-gel process comprise of the following steps (Figure 2.6):

i) Preparation of a homogeneous solution either by using organic solvent miscible with water to dissolve metal organic precursors, or by dissolution of inorganic salts in water,

ii) transformation of the homogeneous solution to a sol by conducting of suitable reagent (generally water with or without any acid/base),

iii) aging,

iv) shaping,

v) thermal treatment/ sintering.

The first step of the sol-gel reaction is the transformation of the molecular precursor into a highly crosslinked solid which is called hydrolysis and condensation reactions. During hydrolysis reactions colloidal particles are dispersed in a liquid and then by condensation reactions a gel formed. This gel formation is interconnected, rigid and porous inorganic network which is enclosed continuous liquid phase. These all reactions are called sol-gel transition. The materials can be produced in various desired shape as monoliths, films, fibers, and monosized powders with sol-gel method. Also some products of sol-gel process can be converted into a ceramic material by heat treatment, (Niederberger & Pinna, 2009).

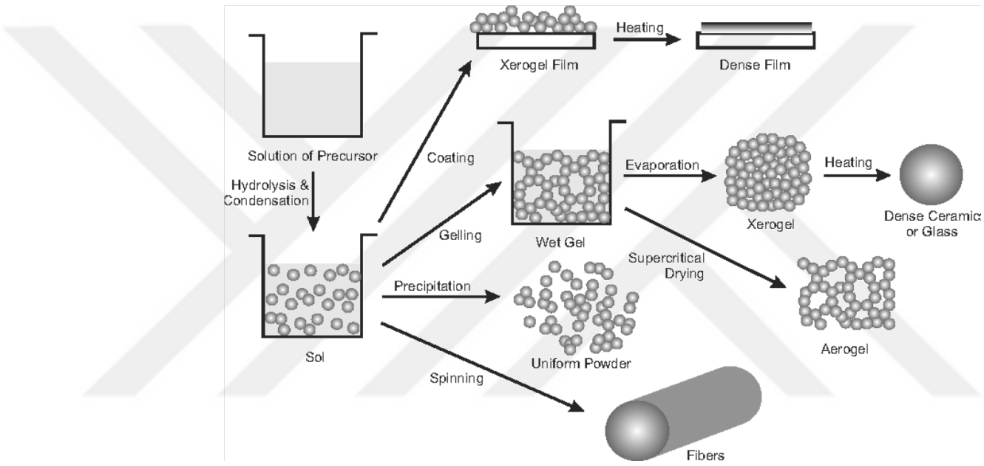


Figure 2.6 Various steps in the sol-gel process to control the final morphology of the product (Niederberger & Pinna, 2009).

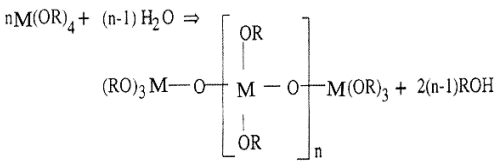
2.3.1 The Chemistry of Precursors Solution

If inorganic sols and gels can be obtained by various methods, they are often directly synthesized from chemical reactants dissolved in a liquid medium. The chemical reactants which contain the cation M (metal) present in the final inorganic sol or gel is called the chemical precursor. Its chemical transformations are complex and involve a competition at the molecular level between the reaction responsible for the formation of open structures and the one leading to dense solid. Those same reactions are responsible for the controlled dispersion of dense colloidal particles in a sol or their agglomeration into a gel (Pierre, 2013).

The metallic salts and the alkoxides can be used as precursor materials. For thin film production metal alkoxides are better than its salts as a precursor to acquire in hole free, crack-free, homogeneous and textured films. Solvents which dissolve precursor have a molecular structure characterized both by a permanent dipole moment μ and by a relative dielectric constant ε_r. A high relative dielectric constant (ε_r>40) is often due to the existence of a permanent dipole moment. Such molecules have good ionizing properties and can therefore dissolve other polar solute. On the other hand when the solvent's relative constant is low (ε_r<20), it has a weak ionizing property and can only dissolve less polar solute. Sol-gel precursors undergo chemical reaction with solvents and the other species present in the solution. One of the most efficient models used to predict those reactions is the Partial Charge Model. Various atomic or molecular groups called ligands can bind to a complex C or cation M either directly or by substituting another ligand. The mechanism of the transformation depends on the partial charge of the different atoms in the species. Those with a negative partial charge are nucleophilic, and those with a positive charge are electrophilic. Similarly, in a substitution reaction, the new ligands with the highest partial charge are the 15 nucleophile while the group in the metal complex with the highest positive charge is the leaving group (Pierre, 2013).

2.3.2 Hydrolysis and Condensation Reaction

Hydrolysis can be expressed by deprotonation of a solvated M cation and it consists in the loss of a proton by one or more of the water molecules that surrounds the M in the first solvation shell during hydrolysis process. As a consequence, the aqua ligand molecule, H_2O that is bonded to the metal is either transformed into an hydroxoligand, OH^-, if only one proton leaves, or into an oxo ligand O^{-2}, if two protons detaches.



(Hydrolysis) (2.1)

After hydrolysis, condensation reaction occurs to form a polynuclear complex consisting of two metal atoms. Condensation, in aqueous solutions, is the result of either an olation or an oxolation reaction. In either case, one must be quite careful as the oxygen present sometimes speeds the reaction to a point where it becomes necessary to work in the neutral atmosphere of argon in order to control it (Pierre, 2013). In the first case, transfer of the H to an OR ligand according to the reaction below (olation process);

$$2M(OR)_{x-1} \longrightarrow (OH)M_2O(OR)_{2X-3}OH + ROH \text{ (Condensation)} \quad (2.2)$$

In the second case, transfer of the H to an OH group according to Reaction (2.3), condensation is called oxolation.

$$2M(OR)_{x-1}(OH) \longrightarrow M_2O(OR)_{2X-3}+H_2O \text{ (Condensation)} \quad (2.3)$$

Hydrolysis and condensation both keep on going thus gradually building up a tridimensional network that, at the end, often forms a solid phase. This process is accelerated by heat as the rate of the both reactions increases together with the temperature. Since the kinetics of hydrolysis and condensation, and hence the overall reaction and the type of polymers formed, depends on the pH, a great variety of materials with different structures can be obtained. These include linear polymers as well as dense colloidal particles and smaller ones with more or less weakly bonded cross-linked clusters of polymers (Pierre, 2013).

2.3.3 Gelation

The gelation point of any system is easy to observe qualitatively and easy to define in abstract terms but extremely difficult to measure analytically. As the sol particles grow and collide, condensation occurs and macroparticles form. The sol becomes a gel when it can support a stress elastically. This is typically defined as the gelation point or gelation time, t_{gel}. There is not an activation energy that can be measured, nor can one precisely define the point where the sol changes from a

viscous fluid to an elastic gel. The change is gradual as more and more particles become interconnected. All subsequent stages of processing depend on the initial structure of the wet gel formed in the reaction bath during gelation (Bevins & Zasloff, 1990).

2.3.4 Drying and Sintering

Drying is irreversible transformation of the gel which is composed of a solid network and liquid matrix. The capillary mechanism explains well the reproducible adsorption hysteresis curves of water in silica gels. This mechanism can be summarized as follows:

- Evaporation creates a liquid vapor meniscus at the exit of pores in the gel.
- This induces a hydrostatic tension in the liquid, which is balanced by an axial compression on the solid.
- The latter compression makes the gel shrink.
- As a result of shrinkage, more liquid is fed to the menisci at the exit of the gel pores, where it is evaporated and so on (Pierre, 2013).

The specific surface area of the porosity is an evolution named sintering. Sol-gel ceramics just after drying and even after heat treatments at intermediate temperatures often have a very high specific surface area and an extremely small grain size. Since states with a lower Gibbs free energy are more stable at a given temperature and pressure, the specific surface area should tend to decrease, an evaluation which can proceed according to two types of pore evaluation: (a) by changing the shape of pores but not their volume and (b) by eliminating the pores. Hence, the dense materials can be obtained after the sintering process (Pierre, 2013).

CHAPTER THREE
NICKEL AND NICKEL MATRIX NANOCOMPOSITE COATINGS

3.1 Nickel Coating

Nickel is an engineering material that is broadly used as electrodepositing material due to the its hardness, high brightness and high corrosion resistance ability (Rostami et al., 2013). Rose and Whittington say that 150,000 tonnes of electroplated nickel was commercially used every year all around the world. This widespread used reflects the useful properties of nickel as a coating and its versatility. The properties and appearance of nickel could be customized to meet specific needs by modifying the composition of the electrolyte and the operating conditions (Rose & Whittington, 2002).

First practical formulation for nickel plating was developed by Bottger in 1843. It was an aqueous solution of nickel and ammonium sulfates. However, there can be an earlier reference which was nickel coating on the platinum electrode from a solution of nickel chloride or sulfate issued by Bird in 1837. After Bird, Shore patented a nickel nitrate solution in 1840. Solution of Bottger had been used in commercial for 70 years however, and he is acknowledged to be the originator of nickel plating (Di Bari, 2000). First commercialized nickel plating in the United States was belong to Dr. Isaac Adams, Jr., a medical doctor educated at Harvard University and at the E ´ cole de Medicine in Paris, he had a patent for his nickel plating gave his company a virtual monopoly in commercial nickel plating from 1869 to 1886. His patent covered the use of pure nickel ammonium sulfate. Although Adams's solution was similar to Bottger's, the difference was pH value on the operating bath. pH was neutral which is undoubtedly vital for controlling the quality of the nickel deposited, since excessive amounts of ammonia would tend to lower cathode efficiency and embrittle the deposit. Largely as a result of the publicity generated by Adams, nickel plating became known worldwide, and by 1886, the annual consumption of nickel for plating had grown to about 135 metric tons (Dennis & Such, 1993; Dubpernell, 1959).

Especially in the last five decades the progress of nickel electroplating gathered speed. It have been used efficiently for both decorative and functional applications and electroforming (Di Bari, 2000; Rose & Whittington, 2002).

Combination of electroplated nickel with electrodeposited chromium is most often applied in decorative applications. The object of the chromium layer was prevention of nickel from tarnishing. It was originally deposited on top of a relatively thick, single layer of nickel that had been polished and buffed to a mirror-bright finish. Thanks to progressive of nickel coating technology, it is not necessary to polish prior to chromium plating to get mirror bright. To protect materials from the corrosive conditions multilayer nickel coating which has equal thickness of the single layer provided better result than the single layer. The corrosion performance of decorative, electroplated nickel plus chromium coatings has been further improved by the development of processes by which the porosity of chromium can be varied and controlled on a microscopic scale. Steel, zinc, copper, aluminum, and many other materials can be protected from corrosion using multilayer nickel coating combined with micro discontinuous chromium for extended periods of time. Nickel and chromium combinations are capable to improve corrosion resistance without increasing thickness and costs (Di Bari, 2000).

Nickel and nickel alloys are also suitable for functional application such as hydraulic rams, automotive cylinder liners, shock absorbers, drying cylinders or rolls, pistons, rotary engine housing, gear shaft and plumbing fitting where decorative appearance is not required. Instead, nickel and nickel alloys with matte or dull finishes are deposited on surfaces to improve corrosion and wear resistance or modify magnetic and other properties. The properties of nickel electrodeposits produced under different conditions of operation are of particular interest in this connection (Di Bari, 2000).

Generally there are two types of deposition techniques of Nickel. First technique is electroplating which is also referred as electrodeposition. This technique is used to change the surface properties of a metal part by adding a metal coating by the action

of electric current. Negative charged object to be coated is immersed into electrolyte solution. This solution includes a salt of the metal to be deposited. Positive charged metal ions are attracted by negative charged object. Surface pretreatment plays important role to obtain successful adhesion of the surface coating. The surface of the object should be cleaned by chemical and mechanical treatment. Some metals used in electroplating are brass, bronze, copper, aluminum, cadmium, lead, iron, chromium, nickel, zinc and tin as well as precious metals such as silver, platinum, and gold. The coatings type can be varied through changing process parameters such as amperage, residence, temperature, voltage, times and composition baths. Because it is an inexpensive and simple method, electroplating method can be employed in different application field such as automobile industry where, for example, chrome plating is used to enhance the corrosion resistance of metal parts, optic and electronic.

Applications of electroplating are numerous because it is an inexpensive and simple method; it is used in all aspects of electronics, optics, and the automobile industry

In the second technique electroless nickel plating, the process action is purely chemical. Coating is achieved through metal ion exchange using chemical reduction in a hot aqueous solution. The deposit properties of an electroless nickel layer and the performance of the plated component depend upon the phosphorous content, the purity, the substrate, the pretreatment, and the thickness of the coating. Electroless nickel deposits may be heat treated to improve abrasion resistance, increase hardness, and enhance adhesion (Balseal, n.d).

3.2 Types of Electrolytes for Nickel Coating Process

3.2.1 Watts Nickel Bath

The majority of nickel plating solutions are based on the ‘Watts’ formulation developed by Professor Oliver P. Watts in 1916. The Watts electrolyte combines

nickel sulphate, nickel chloride and boric acid. While the proportions may vary according to the application, typical constituents and operating conditions for Watts nickel electroplating solutions is given in Table 3.1. The properties of these baths affect the performance of coatings.

It will be seen that close control of the operating parameters is vital, where these properties are important for the performance of the coating (Rose & Whittington, 2002).

Table 3.1 Typical formula and operating conditions for Watts nickel electroplating solutions (Rose & Whittington, 2002).

lphate ($NiSO_4.6\ H_2O$)	g L^{-1}
loride ($NiCl_2.6\ H_2O$)	L^{-1}
d (H_3BO_3)	L^{-1}
ure	
Current Density	$^{-2}$
n Rate	n h^{-1}

The function of all constituents in the Watts bath is explained below.

Nickel sulfate is the primary source of nickel ions (Ni^{++}) with nickel chloride as a contributing source (Rose & Whittington, 2002). Most of the nickel ion content is contributed by nickel sulfate. This salt is used because it is the least expensive salt of nickel with a stable anion that is not reduced at the cathode, oxidized at the anode or volatized. It is also highly soluble and readily available commercially. Nickel sulphamate solutions are widely used for electroforming because of the low internal stress of the deposits, high rate of deposition, and superior throwing power. The throwing power is the relationship between current distribution and uniformity of coating thickness, as influenced by geometric factors (the shape and relative positioning of the anode and cathode) and by the electrochemical characteristics of the solution (conductivity, cathode polarization and cathode efficiency). Throwing power is a measure of the extent to which a solution will produce deposits that are more uniform than those that would be produced in the absence of cathode

polarization and cathode efficiency effects. The limiting cathode current density for sound nickel deposits is a function of nickel concentration in the cathode film, which in turn depends on the metal ion concentration of the bath itself. The large amount of nickel sulfate now used in Watts bath, not only raises the limiting cathode current density, but also lowers the resistivity, thus improving plate distribution (Sadiku-Agboola et al., 2011).

Nickel chloride has two major functions. It increases solution conductivity thereby reducing voltage requirements and it is important in obtaining satisfactory dissolution of nickel anodes (Rose & Whittington, 2002). Because of the existence of chloride ions in the bath, cathode efficiency and electrical conductivity of the solution is improved. A small amount of nickel chloride is usually enough to minimize anode passivity especially at high current densities (Sadiku-Agboola et al., 2011).

Boric acid has the major function of controlling the pH of the solution. is employed as a weak buffer in a nickel plating solution. In the absence of boric acid as a buffer nickel deposit tends to be hard and pit at ordinary temperatures. So the deposit may crack. Boric acid is obtainable in a very pure and inexpensive form, it is non-volatile and stable, it produces whiter deposits, and it is helpful in its smoothing action on the deposit. It is unique in its cooperative effect with leveling addition agents (Sadiku-Agboola et al., 2011).

The nickel plating solution described by Watts (1916) eventually replaced all others in use up to that time. It remains the basis of most decorative nickel plating processes, and is used for engineering applications and for electroforming. It is operated at elevated temperatures and is capable of being used with high current densities (Donald , 1994).

3.2.2 Sulphamate Nickel Bath

Nickel sulphamate solutions are suitable to use for functional coatings. One of them is electroforming which is discussed below. Typical compositions for sulphamate nickel solutions are given in Table 3.2.

The most considerable advantage of sulphamate nickel solutions is the low internal stress of the deposit. But amount of the chloride content is important to obtain minimum stress. The chloride content should be kept at low value. Alternatively, bromide can be substituted for chloride, to maintain low internal stress (Rose & Whittington, 2002).

Table 3.2 Typical composition and operating conditions for nickel sulphamate electroplating solutions (Rose & Whittington, 2002).

lphamate [$Ni(NH_2SO_3)_2.4H_2O$)]	g L^{-1}
loride ($NiCl_2.6H_2O$)	$^{-1}$
d (H_3BO_3)	
ure	
Current Density	m^{-2}
n Rate	m h^{-1}

3.2.3 Other Electrolyte Types for Nickel Coating Process

There are different type of electrolyte formulation can be employed for particular application. These are fluoborate, all-chloride, all-sulphate, high sulphate, hard nickel and black nickel plating solutions. These processes are generally only used in functional applications (Rose & Whittington, 2002).

Fluoborate bath may be operated at very high current densities. Mechanical properties are similar to the Watts nickel deposits. Disadvantages are high cost and highly corrosive solutions (Rose & Whittington, 2002).

All-chloride bath is an alternative process where high current densities are required. These solutions are also much more corrosive than Watts solutions and

therefore equipment must be carefully selected. Deposits are fine-grained and generally harder than Watts nickel coatings (Rose & Whittington, 2002).

The major use for *all-sulphate bath* is in applications involving the use of insoluble anodes (e.g. in the internal plating of pipes and fittings). The absence of chlorides eliminates the problem of toxic chlorine gas being liberated at the anode. Lead or graphite anodes are commonly employed. It is necessary to replenish the nickel ions and to control the pH through regular additions of nickel carbonate (Rose & Whittington, 2002).

The major feature of *high- sulphate bath* is their good throwing power. They have found limited use as a strike bath over zincate pre-treated aluminium (Rose & Whittington, 2002).

Hard nickel bath provides harder deposits and superior abrasion resistance without the use of organic additives. The higher hardness is achieved through the inclusion of ammonium ions. Close control of pH, temperature and current density is necessary for consistent performance (Rose & Whittington, 2002).

Finally, *black nickel bath* has chiefly been applied for decorative purposes Apart from some limited use on optical equipment or for solar collectors. The coatings produced are only thin. Therefore, black nickel is usually applied over satin or bright nickel, and coated with a lacquer or other organic finish (Rose & Whittington, 2002).

3.3 Nanocomposite Coating

Nanostructured coating have been focused by scientist because of their potential of the producing of new material possessing unique physical and chemical properties (Andrievski, 2001; Holubar, Jilek & Sima, 2000; Musil, 2000; Vaz & Rebouta, 2001). Nanostructured coatings lead to be obtain highly complex surface related properties, such as optical, magnetic, electronic, catalytic, mechanical, chemical and tribological properties. With this respect nanostructured coatings became attractive

for industrial application in high speed machining (Veprek & Argon, 2001; Vepřek & Reiprich, 1995), optical applications (Gusev, 1998; Maya, Allen, Glover & Mabon, 1995), tooling (Provenzano & Holtz, 1995; Veprek & Argon, 2001), and magnetic storage devices (Andrievski & Glezer, 2001; Cantor et al., 2001; Mazaleyrat & Varga, 2000) because of their special mechanical, electronic, magnetic and optical properties due to size effect. Different kind of nanostructured coatings such as nanocomposite coatings, nano-scale multilayer coating, superlattice coating, nano-graded coatings, etc. were designed for different purposes. Nanocomposite coatings and materials are among the most exciting and fastest-growing areas of research; with new materials being continually developed which often exhibit novel properties that are absent in the constituent materials. Because of its rapid developing nanocomposite materials and coatings exhibit huge potential for new applications including: aerospace, automotive, electronics, biomedical implants, non-linear optics, mechanically reinforced lightweight materials, sensors, nano-wires, batteries, bioceramics, energy conversion and many others (Öchsner, 2009).

A nanocomposite coating is composed of two or more immiscible phases, of which at least one is restricted to the nanometer scale (1 nm = 10^{-9} m) in at least one dimension. Therefore, a nanocomposite coating is formed by a matrix where filler nanostructures are dispersed (Wang & Chung, 2013).

It is possible to classify nanocomposite regarding to type of nanostructured fillers (Figure 3.1). This classification is formed depend on dimensions of nanostructure in nanometer range. However, the size of this range is not clear. As depicted before, the structures are smaller than 100 nm could be considered as nanoscale structure. The terminology indicates the number of dimensions out of the nanometer range, that is, the real dimensions of the nanostructure are considered to be 3-N, N being the dimensions included in the nanometer range (Wang & Chung, 2013). Taking this into account, three main groups of nanocomposites can be found. First one of this group is 0D-nanocomposites. In this group composite include nanostructure which is in nanometer scale in three dimensions such as nanoparticles. The shape of the nanoparticles is not necessarily spherical. The second group of the nanocomposite is

1D-nanocomposites which include nanotubes or whiskers as fillers (two dimensions in the nanometer range). The last one is 2D-nanocomposites. The fillers in this group are nanolayers (one dimension in the nanometer range).

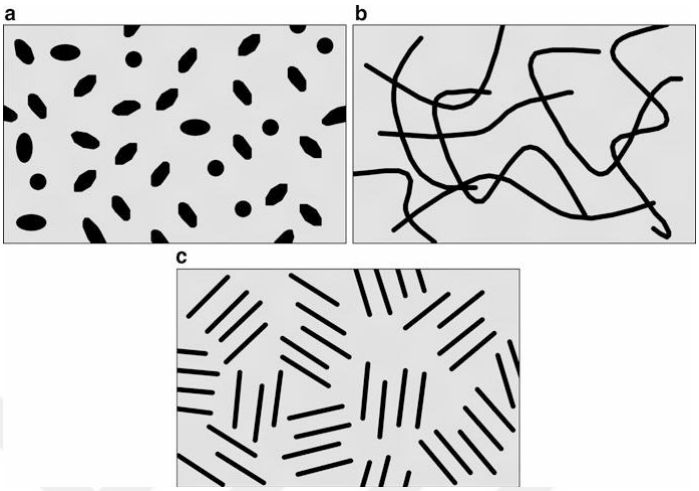


Figure 3.1 Scheme of the different types of nanocomposites. (a) 0D, formed by nanoparticles. (b) 1D, formed by nanotubes. (c) 2-D, formed by nanolayers. The matrix is represented by a gray background (Wang & Chung, 2013).

The properties of a nanocomposite coating depend on the chemical nature of their phases, their relative proportion, and the size of the filler. These properties do not necessarily follow the rule of mixture (i.e., certain properties of a nanocomposite can be improved with respect to those of each component alone). This kind of synergic effect is obtained by a proper control of the structure of the nanocomposite. These films are mainly used with protective applications due to the combination of good corrosion resistance (Baghery et al., 2010), good mechanical properties (high hardness and toughness) and excellent tribological performance (low friction and wear) in different test conditions (Wang & Chung, 2013).

Camargo says “Nanocomposite materials have emerged as suitable alternatives to overcome limitations of microcomposites and monolithics, while posing preparation challenges related to the control of elemental composition and stoichiometry in the nanocluster phase. They are reported to be the materials of 21st century in the view of possessing design uniqueness and property combinations that are not found in

conventional composites. The general understanding of these properties is yet to be reached, even though the first inference on them was reported as early as 1992" (Camargo, Satyanarayana & Wypych, 2009).

Nanocomposite materials can also be classified, according to their matrix materials, in three different categories ceramic, metal and polymer matrix nanocomposite as shown in Table 3.3.

Table 3.3 Different types of nanocomposites (Camargo et al., 2009).

	Examples
	$)_3$, Ni/Al_2O_3, Co/Cr, Fe/MgO, Al/CNT, Mg/CNT
	$_2$, SiO_2/Ni, Al_2O_3/TiO_2, Al_2O_3/SiC, Al_2O_3/CNT
	stic/thermoset polymer/layered silicates, polyester/TiO_2, polymer/CNT, polymer/layered double hydroxides

3.3.1 Ceramic Matrix Nanocomposites (CMNC)

In this group of composites the matrix are ceramic nanostructures, for instance oxides, nitrides, borides, silicides etc.. In general ceramic matrix nanocomposite include metal fillers as the second component. Both metallic and ceramic components are well dispersed in each other to obtain particular nanoscopic properties. With this respect new and unique optical, electrical and magnetic properties (Kruis, Fissan & Peled, 1998) as well as tribological, corrosion-resistance and other protective properties can be obtain (Zhang, Sun, Fu & Du, 2003). There are numerous method to prepare ceramic matrix nanocomposites. These methods can be sorted as; conventional powder method, polymer precursor route, spray pyrolysis, vapour techniques (CVD and PVD) and chemical methods, which include the sol-gel process, colloidal and precipitation approaches and the template synthesis (Camargo et al., 2009).

3.3.2 Metal Matrix Nanocomposites (MMNC)

Metal matrix nanocomposites can also be defined as reinforced metal matrix composites (Bakshi, Lahiri & Agarwal, 2010). Metal matrix composites (MMCs)

include ductile material as a matrix material. These materials can serve at higher temperature than their base metal component. The filler in the composite structure can improve some mechanical properties of the material such as specific stiffness, specific strength, abrasion resistance, creep resistance, thermal conductivity, and dimensional stability (Callister & Rethwisch, 2012). The most common techniques for the processing of metal matrix nanocomposites are spray pyrolysis, liquid metal infiltration, rapid solidification, vapour techniques (PVD, CVD), Electrodeposition and Chemical methods, which include colloidal and sol-gel processes (Camargo et al., 2009).

3.3.3 Polymer Matrix Nanocomposites (PMNC)

In this class of composites polymers are employed as a matrix material and appropriate nanoparticles are added in the polymer matrix. By this way the performance of polymer can dramatically be enhanced. The strategy is specifically effective in yielding high performance composites provided that the fillers are well dispersed in the polymer and filler are substantially different or better than those of the matrix (Manias, 2007). Researchers have used different method to prepare polymer matrix nanocomposite including layered materials and those containing CNTs. The most preferred methods are; i) In-situ intercalative polymerization, ii) Direct mixture of polymer and particulates, iii)Intercalation of the polymer or pre-polymer from solution, iv) Template synthesis, v) Melt intercalation, vi) Sol-gel process, vii) In-situ polymerization (Camargo et al., 2009).

3.4 Nickel Matrix Nanocomposite Coatings

As it mentioned in previous chapter nickel electrodeposition is widely preferred to improve surface properties like corrosion resistance and physical appearance. Unfortunately, the physical and chemical properties of nickel-plated surface such as hardness, corrosion resistance and wear resistance are not as good as required. Different methods were developed to overcome these problems for instance additive of non-metal content (Parida et al., 2011).

With the increasing availability of nanoparticles, the interest in the low-cost and low-temperature composite electroplating is continuously growing, with the major challenge being the achievement of high co-deposition rates and homogenous distribution of the particles in the metallic matrix. Nanoparticles in the metal matrix lead to enhance the mechanical properties and also they have considerable potential to use in high-tech devices. Furthermore, finely dispersed nanoparticles have positive effect in wear and corrosion resistance by hardening of the metal matrix. Nanoparticles prevent movements of dislocations and recrystallization procedures at elevated temperatures. So that, microhardness and thermal stability increase significantly (Karbasi, Yazdian & Vahidian, 2012).

For nickel matrix electrodeposits in particular, a wide variety of particles such as hard oxides (SiO_2, Al_2O_3, TiO_2) (Spanou, Pavlatou & Spyrellis, 2009; Thiemig & Bund, 2008), carbides like (WC and SiC) (Hou, Ger, Wang & Ke, 2002; Kim & Yoo, 1998; Stroumbouli, Gyftou, Pavlatou & Spyrellis, 2005), liquid containing polymeric microcapsules (Kentepozidou, Kiparissides, Kotzia, Kollia & Spyrellis, 1996), carbon nanotubes (Guo, Zuo, Zhao, Zhao & Xiong, 2008), lubricating particles (e.g. MoS2, PTFE and graphite (Cg) (Rostami et al., 2013)) etc. have been used (Karbasi et al., 2012). Furthermore, a number of researchers have been studied on synthesis of Ni based nanocomposites by electrodeposition like Ni–SiC (Ger, 2004; Kim & Yoo, 1998; Niu et al., 2007), Ni-P-SiC (Chou, Ger, Ke, Huang & Wu, 2005), Ni-Al_2O_3 (Borkar & Harimkar, 2011), Ni-ZrO_2 (Borkar & Harimkar, 2011; Rostami et al., 2013).

Recently, Ni-TiO_2 composite coatings have been extensively studied by many researchers. The semiconducting TiO_2 particles attribute the mechanical and optical properties of nickel coating. For example, nickel coating with TiO_2 particles show photocatalytic future. The TiO_2 particles also increased friction resistance, hardness and improved high temperature properties of the coating. (Parida et al., 2011). Baghery and his colleagues produced Ni-TiO_2 nanocomposite coatings using TiO_2 nanopartiles in Ni plating bath by electrodeposition technique. According to their results the microhardness, corrosion resistance and wear resistance of the

nanocomposite coatings increase with increasing of TiO_2 nanoparticle content in the coating (Baghery et al., 2010).

Yan and his friends fabricated Ni-SiO_2 nano-composite coatings by electrodeposition on the AZ91HP magnesium alloy surface, in which nano-SiO_2 was chosen as the second-phase particulates. The results indicate that the Ni-SiO_2 nano-composite coatings with uniform crystalline, dense structure can be obtained on AZ91HP magnesium alloy. The frication and wear experiments reveal that the wear resistances of nano-composite coatings are improved obviously as compared to magnesium alloys and pure nickel coatings (Yan, Yu, Liu, Han & Yuan, 2011). Sadreddini and his colleagues investigate the influences of different concentrations of SiO_2 nano sized particles in the bath on corrosion behavior of Ni-P-SiO_2 composite coatings. According to their research Ni-P-SiO_2 nano-composite coating possesses less porosity than that in Ni-P coating, resulting in improving corrosion resistance (Sadreddini & Afshar, 2014).

Shibli and his colleagues focused on significant improvement of the plate by incorporation with ZnO as a composite in the electroless nickel phosphorus (EN) plate. In the present study, ZnO was selected for the composite plating by virtue of its properties like semi conductivity (band gap of 3.37 eV), piezoelectric property and biocompatibility. The composite plate corresponding to 0.50 g/l of ZnO in the bath showed excellent mechanical as well as electrochemical characteristics (Shibli, Jabeera & Anupama, 2006).

3.5 Production of Nickel Matrix Nanocomposite Coatings

Different techniques are now available for preparation of nanocomposite coatings (Zhang et al., 2003). The most popular among these methods are electrodeposition, chemical vapor deposition (CVD), physical vapor deposition (PVD), ion implantation, laser beam deposition, plasma and high-velocity oxygen fuel (HVOF), sol-gel technique (Ali & Najmy, 2013; Rostami et al., 2013). For instance, Avril and his friends prepared nanocomposite films composed of gold nanoparticles (AuNPs)

embedded in a TiO_2 matrix by direct liquid injection chemical vapor deposition process (Avril et al., 2015). In another study, $NiO–SiO_2$ nanocomposite thin films were prepared by sol–gel technique by Ali and his colleagues (Ali & Najmy, 2013).

The most of the methods mentioned above was explained in Chapter 2 detailly. So only electrodeposition method will be explained in this chapter.

3.5.1 Electrodeposition Method

There are various technique to produce nanocomposite coating were mentioned at previous sections. Electrochemical deposition from aqueous electrolyte solutions gained importance as an attractive and versatile surface finishing technique, due to remarkable advantages such as precise control, uniform deposition, simplicity, low cost in production of large area samples, good reproducibility, versatility, high deposition rate, uniformity of thickness, high purity, low porosity, capability to coat complex component geometries, reduction of waste, easy control of microstructure, and chemical composition of the deposits (Ahmad & Mohamed, 2014; Beltowska-Lehman, Indyka, Bigos, Szczerba & Kot, 2016).

With electrodeposited method, it is also possible to add nanoparticles into the coating structure (Spanou et al., 2009). The process of particle incorporation in the metal matrix during electrodeposition may be described through the following steps:

- Particles transfer from the bulk of the solution to the metal surface
- Interaction i.e. adsorption of particles with the electrode surface
- Particle embedding in the growing metal matrix (Figure 3.2)

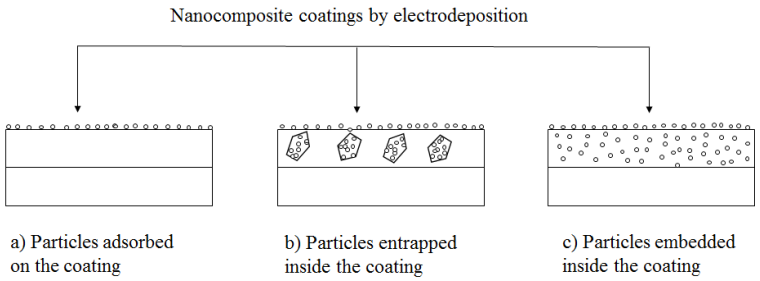


Figure 3.2 Schematic representation of different deposition possibilities

Guglielmi proposed first model of electrodepositing of metal reinforced with particles. This mechanism of the electrodepositing consists of two steps. Firstly, weak Van der Waals forces with high degree of surface coverage which can be presented by Langmuir adsorption isotherm lead to be adsorbed particles on the cathode surface. In second step of the electrodeposition process due to strong Coulomb forces under the effect of applied electric field particles are strongly adsorbed on the surface and these particles are incorporated in the growing metal matrix. According to this model the volume fraction of the incorporated particles, α, can be expressed as:

$$\frac{\alpha}{1-\alpha} = \frac{zF\rho_m V_0}{M_m i_0} \cdot e^{(B-A)\eta} \cdot \frac{kc_b}{kc_b+1} \tag{3.1}$$

where M_m and ρ_m are the atomic weight and the density of the deposited metal, respectively, i_o is the exchange current density, z is the valence of the electrodeposited metal, F is Faraday constant, η is the electrode overpotential, c_b is the bulk concentration of particles and k is the Langmuir adsorption constant. The main drawback of this model is that it neglects the particle size, hydrodynamics i.e. mass transfer of particles.

Ahmad says “Celis proposed a five-step mechanism to account for the electrocodeposition process: (i) formation of ionic cloud around the particles; (ii) mass transfer of particles by convection to the hydrodynamic boundary layer; (iii) mass transfer of particles to the cathode surface by diffusion; (iv) adsorption of free ions and electroactive ions adsorbed on the particles on the cathode, and (v) electro-

reduction of adsorbed ions accompanied with incorporation of particles into the growing metal matrix".

According to Kurozaki study, dispersed particles are transferred to the Helmholtz's double layer by mechanical agitation in the first step. Secondly, particles which are charged in the high potential gradient are transferred to cathode by electrophoresis. In the third step, particles are adsorbed on the cathode surface by coulomb attraction between them and adsorbed anions on the cathode and hence are incorporated into the growing metal layer. Other models were suggested by authors but still more work is needed that accounts more with the particle characteristics (composition, size, crystallinity, etc.) and the operating electrodeposition parameters (Ahmad & Mohamed, 2014).

Principle of electrolysis process is reducing the cations of a desired material from an electrolyte and coats those materials as a thin film onto a conductive substrate surface using electrical current. Figure 3.3 shows a simple electrodeposition system for nickel chloride solution (Saidin, Ying & Khuan, 2011).

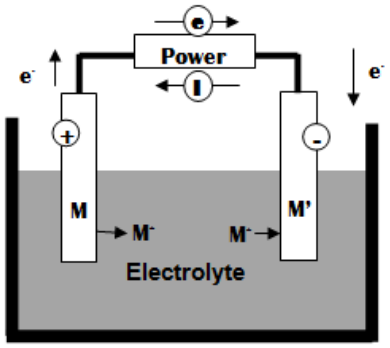


Figure 3.3 Simple electrodeposition system (Saidin et al., 2011).

The electrolyte solution contains positively charged nickel ions (cations) and negatively charged chloride ions (anions). Under an applied external electric field, the cations migrate to the cathode where they are discharged and deposited as metallic nickel.

$$Ni^{2+} + 2e \leftrightarrow Ni \text{ (metal)} \quad (3.2)$$

Nickel from the anode dissolves into the solution to maintain the electrical neutrality.

$$Ni \leftrightarrow Ni^{2+} + 2e \quad (3.3)$$

The overall process is known as electrolysis. Noble metal, platinum plate, is used as the anode. The reaction occur at the anode is the oxidation of water.

$$2H_2O \leftrightarrow 4H^{+} + O_2 + 4e \quad (3.4)$$

The chloride ions remain unchanged in quantity during the electrolysis but the concentration of Ni^{2+} ions will decrease and that of H^{+} ions will increase with time as the noble metal is used as the anode in this work.

Under the influence of an applied potential, rearrangement of ions near the electrode surface results in an electrical double layer called Helmholtz double layer, followed by the formation of a diffusion layer (Figure 3.4). The process is as follows:

- Migration – the hydrated metal ions in the solution migrate towards the cathode under the influence of impressed current as well as by diffusion and convection.
- Electron transfer – at the cathode surface, a hydrated metal ion enters the diffused double layer where the water molecules of the hydrated ion are aligned. Then the metal ions enter the Helmholtz double layer where it is deprived of its hydrate envelope.
- The dehydrated ion is neutralized and adsorbed on the cathode surface.
- The absorbed atom then migrates or diffuses to the growth point on the cathode surface (Saidin et al., 2011).

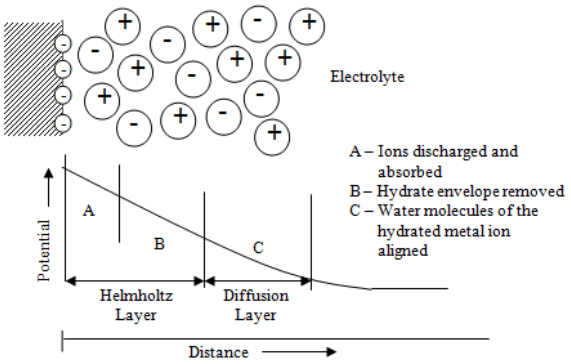


Figure 3.4 Electrical double layer (Saidin et al., 2011).

Several parameters can influence the electrodeposition process and consequently the microstructure of the composite coating, these parameters include:

- the electrolysis conditions
  - composition of the electrolyte bath,
  - Solution concentration
  - presence of additives,
  - pH,
  - temperature
  - electrolyte agitation,

- current conditions
  - type of imposed current,
  - values of current density,

- the properties of the reinforcing particles
  - size,
  - surface properties,
  - concentration and type of dispersion in the bath (Ahmad & Mohamed, 2014) (Karbasi et al., 2012) (Stroumbouli et al., 2005) (Kentepozidou et al., 1996) (Rashidi & Amadeh, 2009) (Saidin et al., 2011).

CHAPTER FOUR
EXPERIMENTAL STUDIES

This study involves preparation of titanium dioxide (TiO_2), zinc oxide (ZnO) and silica (SiO_2) nanoparticles by sol-gel technique. Afterwards Ni matrix nanocomposite coatings deposited by electrodeposition method with different current density, nanoparticles size and concentration.

4.1 Production of Nanoparticles

4.1.1 Production of TiO_2 Nanoparticles

TiO_2 nanoparticles were synthesized by sol-gel method using titanium (IV) isopropoxide, glacial acetic acid and deionized water. Two different types of solutions were prepared in order to produce TiO_2 nanoparticles. First solution (TiO_2-A) was prepared by dissolving titanium (IV) isopropoxide in the glacial acetic acid and deionized water with the molar ratio of 1: 10: 200. Glacial acetic acid acts as a catalyst to prevent titanium isopropoxide from the nucleophilic's attacks by the water (Doeuff, Henry, Sanchez & Livage, 1987). The solution was stirred and dried at about 80 ºC over night. The dried gel was grinded and calcined in a muffle furnace at 500 ºC for 5 hours. The flow chart of the solution preparation (TiO_2-A) is illustrated in Figure 4.1.

Second type solution (TiO_2-B) was prepared by same method as mentioned above. Additional to the mentioned procedure, egg white solution was used as gelling agent. Freshly water-soluble egg white proteins were homogenized in water by stirring on a magnetic stirrer for one hour. Then, the egg white solution was added into the precursor solution. The solution was continued to be heated and stirred at about 80 ºC overnight. The result solution was then dried in the oven at 80 ºC overnight. The dried gel was grinded and calcined at 500 ºC for 5 hours (Bagheri, Shameli & Abd Hamid, 2012). The flow chart of the solution preparation (TiO_2-B) is illustrated in Figure 4.2.

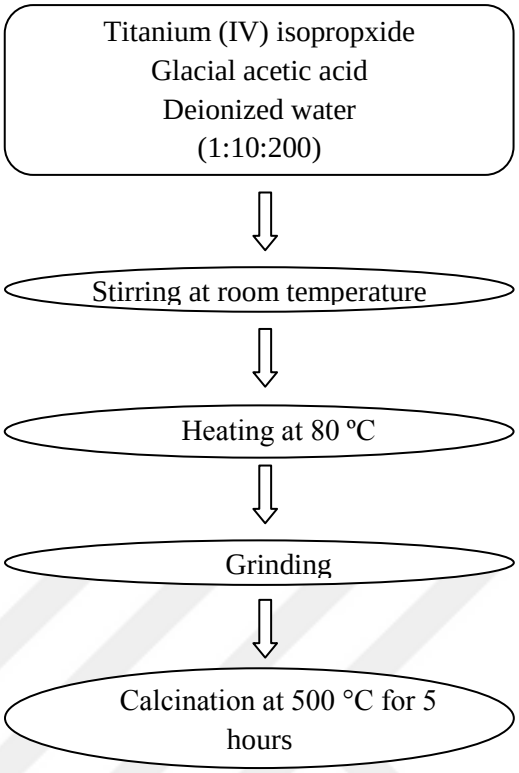


Figure 4.1Schematic illustration of sol TiO_2-A preparation

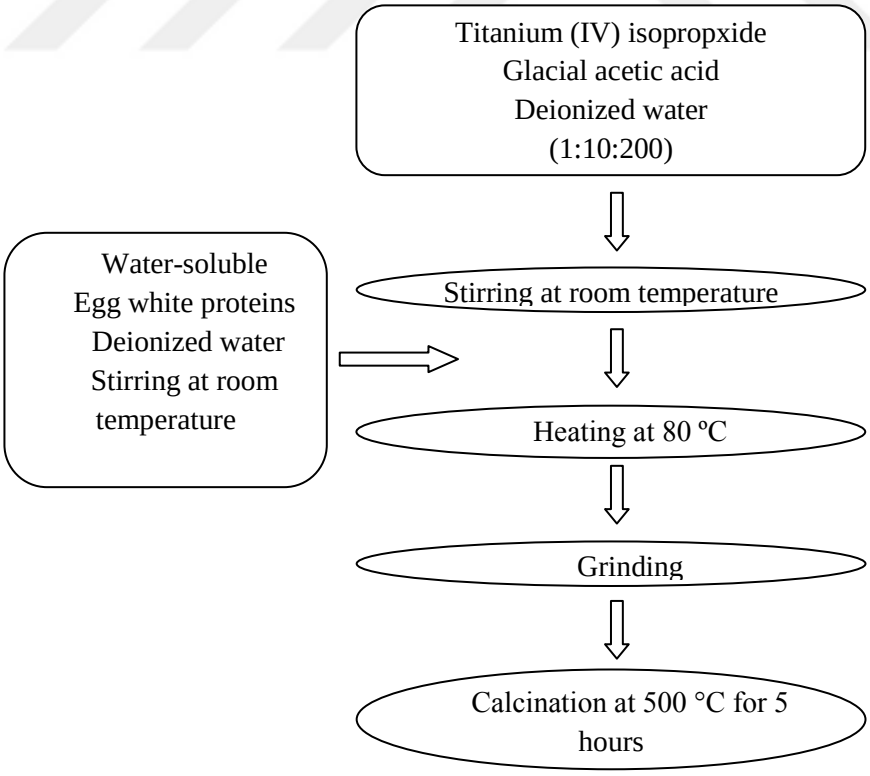


Figure 4.2 Schematic illustration of sol TiO_2-B preparation.

4.1.2 Production of ZnO Nanoparticles

ZnO nanoparticles were synthesized via sol-gel method. Flow chart in Figure 4.3 was created by utilizing from research of Alias and Singh's colleagues. 3 individual ZnO sols having different molarities were prepared by dissolving zinc acetate dehydrate in methanol at room temperature. The solutions were stirred for 2 hours using a magnetic stirrer to obtain transparent solutions. The pH of the sols was found to be 6. Thereafter 1.0 M NaOH was titrated to get 4 different pH values in the each individual sol. The each solution was again stirred for 60 min. All of the samples were left alone several days to allow the sol-gel process to finish. Afterwards, the sols were centrifuged using at 3000 rpm for 30 min to complete gelation and hydrolysis and then the wet, white precipitate of ZnO was dried at 80 °C. Finally, the dried precipitate was ground to fine white powder (Alias, Ismail & Mohamad, 2010; Singh, 2012). As conclusion, different ZnO particles were produced using different parameters such as molarity, pH and waiting time.

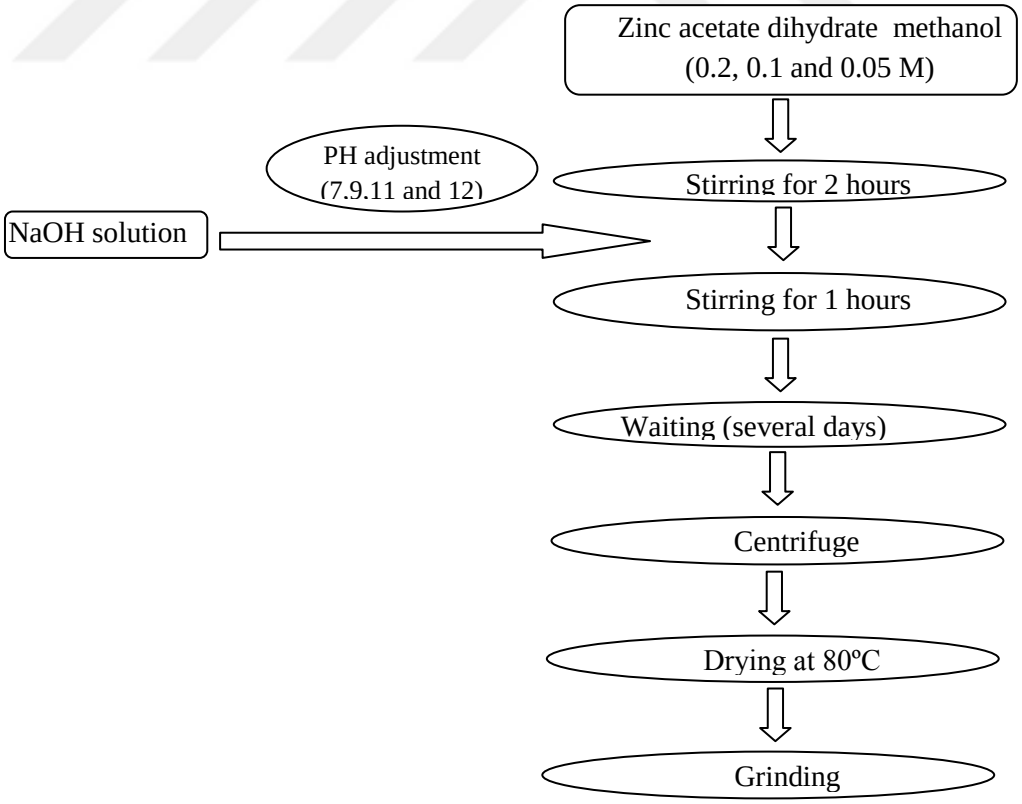


Figure 4.3 Schematic illustration of ZnO nanoparticles preparation by sol-gel technique.

4.1.3 Production of SiO_2 Nanoparticles

Silica nanoparticles were prepared by hydrolysis of tetraethyl orthosilicate (TEOS) in ethanol medium in the presence of ammonium hydroxide. The process of silica nanoparticle synthesis is depicted in Figure 4.4. Firstly 4 M ethanol and 14 M demonized water were mixed and kept in ultrasonic bath. TEOS was added into mixture while sonicating and mixture was sonicated. Thereafter, 14 M 26% ammonium hydroxide was added dropwise as a catalyst to promote the condensation reaction and sonication was continued until white turbid suspension was observed. After the completion of these reactions, the resultant suspension was dried in an oven at 80 °C, accompanied by calcination at 500 °C (Dabbaghian, Babalou, Hadi & Jannatdoust, 2010; Rao, El-Hami, Kodaki, Matsushige & Makino, 2005). All of these processes were repeated for different TEOS molarities such as 0.09 M, 0.045 M and 0.0225 M.

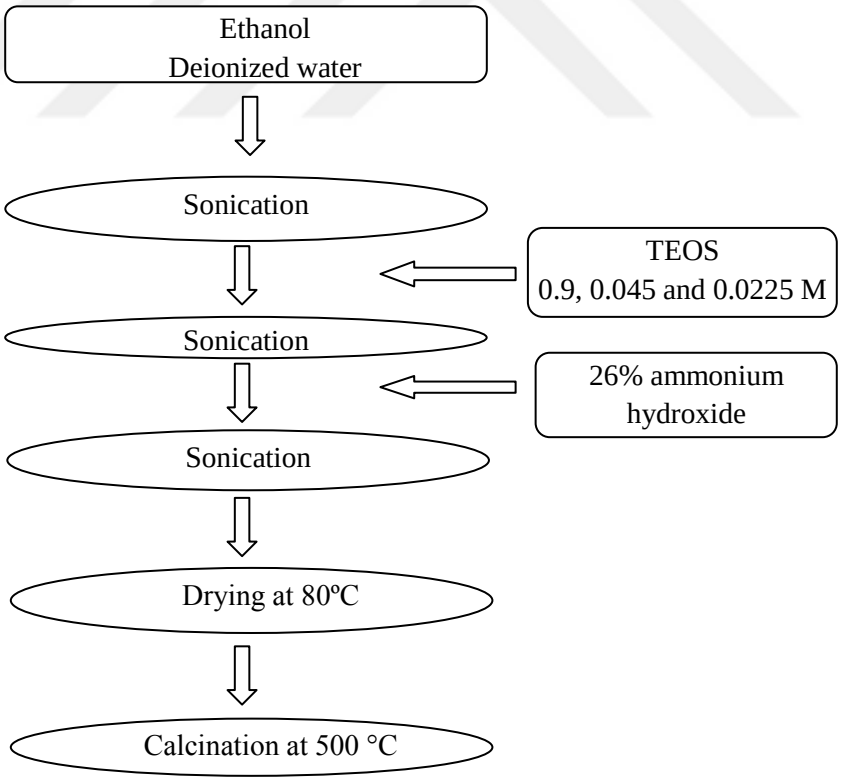


Figure 4.4 Schematic illustration of SiO_2 nanoparticles preparation by sol-gel technique

4.2 Preparation of the Substrate

Steels with dimensions of 100mm×25mm were selected as the substrate material. Firstly steel substrates were mechanically polished using SiC paper up to a grit of 1200. After that, these substrates were pre-treated 60 seconds in etching solution which is given in Table 4.1. Finally they were washed with distilled water and rinsed with ethanol.

Table 4.1Etching solution

Chemicals	Amount (vol%)
Nitric acid (HNO_3)	15
Hydrofluoric acid (HF)	5
Deionized water	80

4.3 Production of Electrodeposited Pure Nickel and Nickel Matrix Nanocomposite Coatings

Pure Ni and Ni matrix nanocomposite coatings were electrodeposited from a nickel Watts type solution. Electrochemical bath components were consisted of nickel sulfate as Ni source, boric acid as buffer solution, nickel chloride to prevent the anode from being passivity and other agents/additives are brighteners, carriers, rectifiers and wetting agents. Deposits from Watts solutions without additives are soft and ductile and dull in appearance. The appearance and properties can be changed by the use of addition agents. The addition agents consist of organic and certain metallic compounds selected to brighten and level the deposits (Rose & Whittington, 2002). TiO_2, SiO_2 and ZnO nanoparticles with particle sizes of ~80 nm and ~50 nm were added into the Watts bath to obtain different types of Ni matrix nanocomposite coatings.

Production of Ni and Ni matrix nanocomposite coatings was carried out on steel substrates having pre-treated surface by electrochemical deposition method in Watts bath using CHROMA 62050P-100-100 power supply. The bath composition and

operating conditions are presented in Table 4.2 and 4.3, respectively. The coatings were named according to applied different current density and time in Table 4.4. The experimental setup is illustrated in Figure 4.5.



Figure 4.5 Experimental setup

Before electrodeposition process, the Watts baths had been stirred for 24 hours to avoid precipitation of particles in the bath and stirring was maintained during electrodeposition process.

Table 4.2 Composition of the electrodeposition bath

Chemicals		**Amount of constituents**
Nickel (II) Sulfate Hexahydrate	$NiSO_4 \cdot 6H_2O$	112.5 g
Nickel (III) Chloride Hexahydrate	$NiCl_2 \cdot 6H_2O$	15 g
Boric Acid	H_3BO_3	15 g
Organic Compound	Ni-Brightener	0.5 ml
Organic Compound	Ni- Carrier	10 ml
Organic acid	Ni- Rectifier	5 ml
Surface Active Agent	Ni- Wetting Agent	0.5 ml
Deionized water		500 ml
Nanoparticle	$TiO_2/SiO_2/ZnO$	1 g/l, 3 g/l

Table 4.3 Overwiew of the electrodeposition parameters of Nickel and Ni matrix nanocomposite coatings

Electrodeposition Parameters	
Particle size of TiO_2/SiO_2/ZnO nanoparticles (nm)	~50, ~80
Concentration of TiO_2/SiO_2/ZnO nanoparticles (g/t)	1, 3
Substrate	SS
Surface modification	Acidic Surface Treatment
Composition of Bath	Fixed
Time (min)	10
Current Density (A dm^{-2})	3, 5, 7
Temperature (°C)	45
Mixing Rate (rpm)	200

Table 4.4 Nomenclature of the coatings according to the deposition parameters

Abbreviation	**Type of Nanoparticle**	**Size of nanoparticle**	**Current Density (A dm^{-2})**
AE10-3	-	-	3
AE10-5			5
AE10-7			7
E50-1T-3	TiO_2	~50 nm	3
E50-1T-5			5
E50-1T-7			7
E80-1T-3		~80 nm	3
E80-1T-5			5
E80-1T-7			7
E50-3T-3		~50 nm	3
E50-3T-5			5
E50-3T-7			7
E50-1Z-3	ZnO	~50 nm	3
E50-1Z-5			5
E50-1Z-7			7
E80-1Z-3		~80 nm	3
E80-1Z-5			5
E80-1Z-7			7
E50-1S-3	SiO_2	~50 nm	3
E50-1S-5			5
E50-1S-7			7
E80-1S-3		~80 nm	3
E80-1S-5			5
E80-1S-7			7
E50-3S-3		~50 nm	3
E50-3S-5			5
E50-3S-7			7

4.4 Characterization of the Nanoparticles and Nanocomposite Coatings

4.4.1 X-ray Diffraction (XRD)

X-ray diffraction refers to a nondestructive analytical method that uses the diffracted intensity of a monochromatic x-ray beam as a function of the incident and exit angle. Information about the crystallographic structure, chemical composition, and physical properties of materials and thin films can be obtained. In addition, precise lattice parameters, crystallite size, preferred orientation, and lattice stress can be calculated.

When monochromatic x-rays impinge on a sample, the x-rays are scattered (diffracted) by atoms in the material. If the atoms in the material have a crystalline structure, this scattering results in maxima and minima in the diffracted intensity distribution (Figure 4.6). The signal maxima follow Bragg's law;

$$n\lambda=2.d.\sin\theta \qquad (4.1)$$

in which n is an integer, λ is the x-ray wavelength, d is the distance between crystal lattice planes, and Θ is the diffraction angle. Thus, for each lattice spacing d, Bragg's law predicts a maximum at a characteristic diffraction angle Θ. When the intensity of the detected x-rays is plotted as a function of the angle Θ, an XRD pattern is obtained that is characteristic for the sample material (Feddes et al., 2009) .

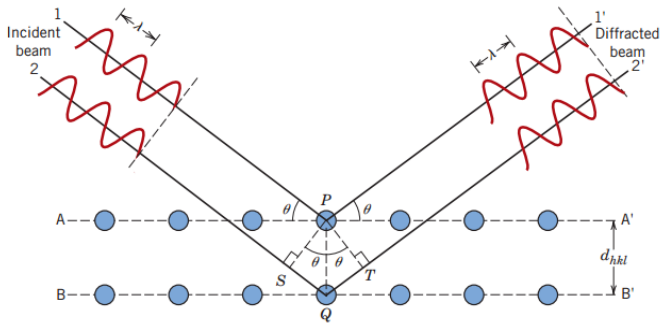


Figure 4.6 Diffraction of x -rays by planes of atoms (A -A ' and B -B ')(Callister & Rethwisch, 2007)

In this study sol-gel synthesized nanoparticles and electrodeposited coatings were analyzed using X-Ray Diffraction (XRD, Rigaku, D/Max-2200/PC) with a grazing incident angle of 1° at 40 kV and 36 mA using Cu K_α radiation with a scanning speed of 4° 2θ/min, from diffraction angle of 3° to 90°.

4.4.2 Particle Size Analyser

A typical particle size analyzer system comprises of six main components. First of all a laser is used to provide a light source to illuminate the sample particles within a cell. Most of the laser beam passes straight through the sample, but some is scattered by the particles within the sample. A detector is used to measure the intensity of the scattered light. As a particle scatters light in all directions, it is (in theory), possible to place the detector in any position and it will still detect the scattering. The intensity of the scattered light must be within a specific range for the detector to successfully measure it. If too much light is detected then the detector will become overloaded. To overcome this an "attenuator" is used to reduce the intensity of the laser and hence reduce the intensity of the scattering. The appropriate attenuator position is automatically determined by the Zetasizer during the measurement sequence. The scattering intensity signal for the detector is passed to a digital signal processing board called a correlator. The correlator compares the scattering intensity at successive time intervals to derive the rate at which the intensity is varying. This correlator information is then passed to a computer, where the specialist Zetasizer software will analyse the data and derive size information.

In this study, Malvern Zeta Sizer Nano ZS90 device is used to determine particle size of TiO_2, SiO_2 and ZnO particles with laser diffraction principle.

4.4.3 Scanning Electron Microscopy (SEM)

Scanning electron microscopy (SEM) is one of the most common analytical methods to analyse surface morphology of the solid-state sample. With SEM, an incident electron beam generated by an electron gun, accelerated by high voltage,

and focused on the sample surface by a series of electromagnetic lenses scans the surface of the sample by means of a series of deflection coils and synchronized with a cathode-ray tube (CRT). The signals produced as a result of the beam interaction with the sample surface are collected by a suitable detector, amplified, and displayed on the CRT.

The energy dispersive spectroscopy (EDS) is often attached to the SEM. The X-rays generated from the interaction between the electron beam and the sample is used to identify and measure quantitatively the elemental composition of the sample. Therefore, SEM/EDS can specify the elemental composition and obtain the morphology of the sample simultaneously.

In this study, the surface morphology and elemental composition of the coatings was examined by using JEOL-JSM 6060 Scanning Electron Microscopy with an Energy Dispersive X-ray spectroscopy (IXRF System EDS) system attachment.

4.4.4 Electrochemical Method

The corrosion measurements of Ni matrix nanocomposite coatings were performed using a Gamry potentiostat/galvanostat system controlled by the Gamry Framework software and Echem Analyst software, for the acquisition and analysis of electrochemical data, respectively. The corrosion measurements were carried out in three electrode cell in 3.5 (% wt) NaCl solution at 25 °C. The Ag/AgCl electrode was used as reference electrode, graphite was employed as counter electrode and prepared samples were used as working electrode in three electrode cell. Electrochemical properties were analyzed to measure corrosion performance of prepared coatings by potentiodynamic measurements. Open circuit potential (OCP) was measured in NaCl solution for 60 minutes. Tafel measurements were carried out between -0.25 V and +0.25 V at 0.1667 mV/s scanning rate. Potentiodynamic measurements were done between 0.5 V lower than OCP value and 0.5 V at 0.5 mV/s scanning rate.

CHAPTER FIVE
RESULTS AND DISCUSSION

5.1 Sol-Gel Synthesized Nanoparticles

5.1.1 Characterization of TiO_2 Nanoparticles

Titanium dioxide held remarkable interest thanks to its unique properties such as easy handling, resistance to photochemical and chemical erosion, non-toxicity, relatively low cost production, superior photocatalytic performance, environmentally friendliness and long-term stability. These useful properties make TiO_2 commercially important and suggest using in industrial applications such as chemical sensors for hydrogen gas evaluation, solar cells, self cleaning surfaces and photocatalytic applications such as environmental purification systems. The oxide nanoparticles synthesized by sol-gel technique appear more and more useful, because of their good electrical, optical and magnetic properties that are different from their bulk counterparts (Ranganathan et al., 2015; Sharmila Devi, Venckatesh & Sivaraj, 2014).

The preparation of TiO_2 colloids in the nanometer range can be effectively carried out through the hydrolysis and condensation of titanium alkoxides in aqueous media. In the presence of water, alkoxides hydrolyze and subsequently polymerize to form a three-dimensional oxide network. These reactions can be schematically represented as follows(Mahshid, Ghamsari, Askari, Afshar & Lahuti, 2006):

$$Ti(OR)_4 + 4H_2O \xrightarrow{\text{Hydrolysis}} 2Ti(OH)_4 + 4ROH, \quad (5.1)$$

$$Ti(OH)_4 \xrightarrow{\text{Condensation}} TiO_2\, xH_2O + (2- x)H_2O \quad (5.2)$$

The X-ray diffraction pattern of sol-gel synthesized TiO_2 nanoparticles was given in Figure 5.1. It is observed that XRD results of TiO_2 nanoparticles were exhibited anatase phase. The 2θ characteristic peaks of anatase TiO_2 at 25.37, 37.91, 48.16, 54.05, 55.20, 62.87, 68.98, 70.48, 75.30, and 82.93 corresponding to the (101), (004),

(200), (105), (211), (204), (116), (220), (215), and (224) planes of the crystal lattice, respectively (Anatase XRD JCPDS Ref. No. 21-1272).

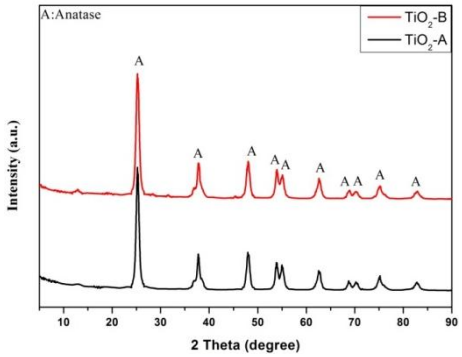


Figure 5.1 X-ray θ-2θ scans of TiO_2-A and TiO_2-B nanoparticles.

In literature it is depicted that common reported qualities of photoactive TiO_2 nanoparticles include high crystallinity, anatase phase material and small particle size. These small providing sufficient exposed titania sites on which photocatalytic reaction can takes place (Shirke, Korake, Hankare, Bamane & Garadkar, 2011).

Mixture that contains 20 ml distilled water and 20 mg TiO_2 nanoparticles were prepared to measure the size of particles using Zeta-Sizer device. Figure 5.2 and Table 5.1 show distribution charts and values of particle sizes, respectively. When the results were examined, it is understood that the particle size was reduced by the addition of egg white solution as an agent. Bagheri and his colleagues synthesized TiO_2 nanoparticles with and without water soluble egg white proteins and confirmed that TiO_2 nanoparticles were synthesized with egg white proteins have smaller than without (Bagheri et al., 2012). Our results are consistence with them. The egg white solution was applied as a stabilizer and gelling agent for reducing agglomeration of TiO_2 nanoparticles. Water-soluble proteins of egg white forms a matrix of entangled polymeric chains, inside the cavities of which can trap small volumes of metal ions. During heat treatment, the dried precursors decompose into nanocrystalline products.

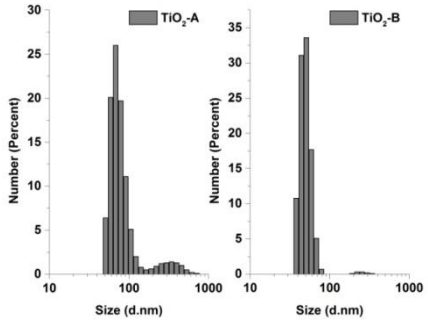


Figure 5.2 Distribution chart of particle sizes of (a) TiO_2-A (without gelling agent), (b) TiO_2-B (with gelling agent).

Table 5.1 Particle size values of TiO_2 nanoparticles

	Particle Size
TiO_2-A	~74.39 nm
TiO_2-B	~49.69 nm

5.2 Characterization of ZnO Nanoparticles

ZnO is a semiconductor which as wide band gap with a large exciton binding energy at room temperature. It shows high transmittance and good electritical conductivity. ZnO could be used in film form for different applications such as transparent electrode for solar cell window and gas sensors. Moreover, because of its stability against photo corrosion and photochemical properties, it shows potential using in solar energy conversion (Rani, Suri, Shishodia & Mehra, 2008)

The ZnO nanoparticles were synthesized using sol-gel process undergoes four stages; solvation, hydrolysis, polymerization and transformation into ZnO nanoparticles. The zinc acetate dehydrate precursor was first solvated in methanol, and then hydrolyzed which results in a colloidal-gel of zinc hydroxide (Eq. 5.3). This zinc hydroxide splits into Zn^{2+} cation and OH^- anion (Eq. 5.4), followed by polymerization of hydroxyl complex to form ‘‘Zn-O-Zn’’ bridges and finally transformed into ZnO (Eq. 5.5) (Singh, 2012).

$$ZnO(CH_3COO)_2.2H_2O+2NaOH \rightarrow Zn(OH)_2+2CH_3COONa+2H_2O \qquad (5.3)$$

$$Zn(OH)_2 + 2H_2O \rightarrow Zn(OH)_4^{+2} + 2H^{2+} \quad (5.4)$$

$$Zn(OH)_4^{+2} \leftrightarrow ZnO + H_2O + 2OH^- \quad (5.5)$$

The X-ray diffraction pattern of ZnO nanoparticles prepared from 0.2, 0.1 and 0.05 M precursor solution with different pH values are shown in Figure 5.3. It is obvious from the figure that the samples prepared at pH 7 have no intense ZnO peak. Normally, the ZnO structure cannot be synthesized well at pH 6 because of the high concentration of H^+ ions and low concentration of OH^- ions in the sol. For the neutral condition at pH 7, the number of H^+ ions reacting with number of OH^- from NaOH is equivalent. Therefore, both of the peaks are broad. The ZnO powder peaks for samples with pH≥8 show the crystalline nature with angles of diffraction (2θ) = 31.68°, 34.35°, 36.16°, 47.45°, 56.48°, 62.74°, 67.84° and 68.96° corresponding to the (100), (002), (101), (102), (110), (103), (112) and (201) planes of the crystal lattice, respectively (JCPDS Ref. No. 36-1451). The highest ZnO intensity peak (2θ = 36.16º) appears at pH 9 because a sufficient amount of OH^- is available to form ZnO (Alias et al., 2010; Singh, 2012).

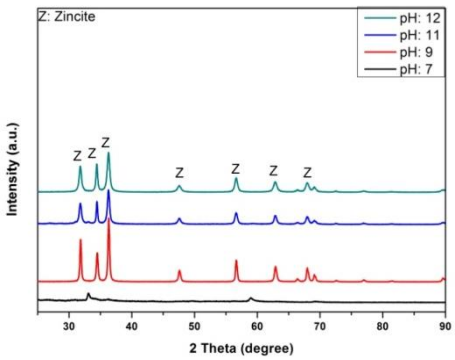


Figure 5.3 X-ray θ-2θ scans of ZnO nanoparticles

Particle size distribution charts of ZnO nanoparticles were synthesized with different molarities and different pH values are shown in Figures 5.4-5.7. It can be understood from Figures 5.4-5.7 that the particle sizes were decreased with increasing pH value up to 11 except particles obtained from 0.1M solution. After this pH point, the particle size values increased again. Table 5.2 which demonstrate

particle size values also revealed that the finest particles were synthesized at 0.05 M and 11 of pH. And then these parameters were fixed and waiting time was reduced from 4 days to 1 day. Figure 5.7 and Table 5.2 are also shows distribution charts and values of particle size at this new waiting time, respectively. Similar studies are observed in literature. Singh and his colleagues synthesized ZnO nanoparticles by sol-gel method. They studied effects of pH variation as well as ageing. The nanoparticles were synthesized with two different pH levels such as pH 7 and pH 10. It was found that the size of the nanoparticles increased with increase in pH level from 7 to 10. Further the effect of ageing on the ZnO nanoparticles was studied. It was found that the crystallite size of the nanoparticles increased with ageing (Singh, 2012).

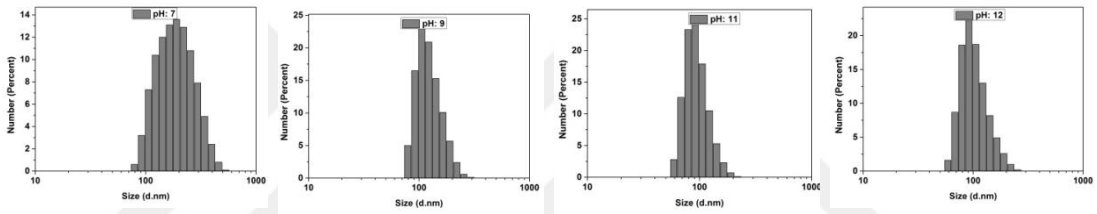


Figure 5.4 Particle size distribution chart of ZnO nanoparticles were synthesized at 0.2 M and pH: 7, 9, 11, 12

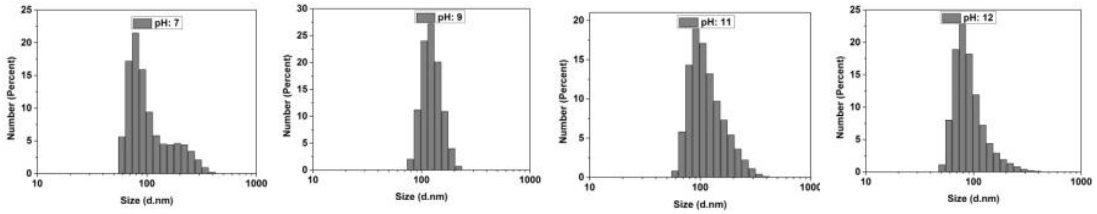


Figure 5.5 Particle size distribution chart of ZnO nanoparticles were synthesized at 0.1 M and pH: 7, 9, 11, 12

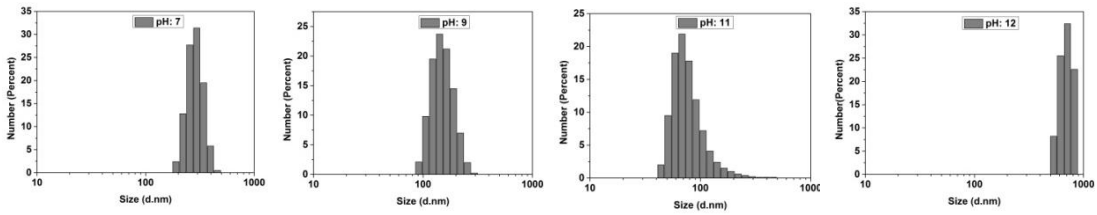


Figure 5.6 Particle size distribution chart of ZnO nanoparticles were synthesized at 0.05 M and pH: 7, 9, 11, 12

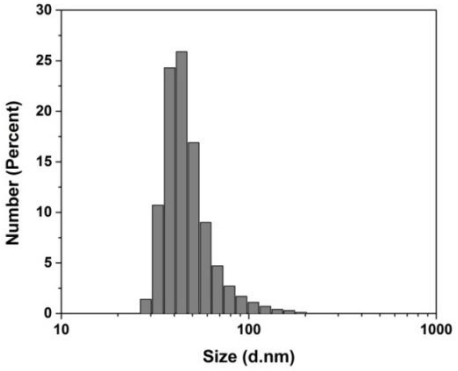


Figure 5.7 Particle size distribution chart of ZnO nanoparticles were synthesized at 0.05 M, pH: 11 and waiting time: 1 day

Table 5.2 Particle size value of ZnO nanoparticles

Molarite	Waiting time	pH7	pH9	pH11	pH12
0.2	4 days	197.9	125.5	95.63	105.2
0.1	4 days	~91.46	125.9	122	95.66
0.05	4 days	287.8	153.3	81.67	728
0.05	1 days	-	-	48.60	-

5.3 Characterization of SiO_2 Nanoparticles

Advancement in nanotechnology has led to the production of nano sized silica. Due to the its low density, good mechanical and thermal stability, chemical inertia, easy preparation, SiO_2 is widely used in various industrial applications such as catalysis, pigments, pharmacy, electronic and thin film substrates, electronic and thermal insulators, and humidity sensors (Gorji, Ghasri, Fazaeli & Niksirat, 2012; Rahman & Padavettan, 2012; Rao et al., 2005).

Sol-gel process has proven to be a promising method for preparing monodispersed, nanosized, spherical silica particles using tetraethylorthosilicate (TEOS) as a precursor due to its simplicity and cheapness. It involves hydrolysis followed by polycondensation of the precursor under alkaline conditions. Through this technique, silanol groups are produced via the former process shown by reaction (5.6), which acts as a substrate for reaction (5.7), leading to a three-dimensional

cross-linked network structure as a result of the latter process due to the formation of siloxan bridges (Si-O-Si) (Dabbaghian et al., 2010).

$$Si(OC_2H_5)4+4H_2O \xrightarrow{\text{Hydrolysis}} Si(OH)_4+4C_2H_5OH \quad (5.6)$$

$$Si(OH)_4 \xrightarrow{\text{Condensation}} (\text{-Si-O-Si-})+H_2O \quad (5.7)$$

Figure 5.8 shows the X-ray diffraction pattern of SiO_2 nanoparticles. The powder diffraction pattern indicates a broad peak at $2\theta = 22^{\circ}$, which reveals the amorphous nature of the silica nanoparticles (JCPDS Ref. No. 01-075-0638). Further, the XRD pattern confirms the absence of any ordered crystalline structure. Music and Dabbaghian and their colleagues synthesized SiO_2 nanoparticles using sol-gel method. SiO_2 nanoparticles which obtained from these works have an amorphous peak was centered at $2\theta = 22^{\circ}$ (Dabbaghian et al., 2010; Musić, Filipović-Vinceković & Sekovanić, 2011).

The distribution charts and values of particle sizes of SiO_2 nanoparticles which were synthesized using different molarities shows in Figure 5.9 and Table 5.3, respectively. Distribution charts of SiO_2 particle sizes demonstrate that the particle size decrease with decreasing of TEOS molarities. This situation can be related to mechanism which raising [TEOS]/[H_2O] ratio enhances the probability of the monomer addition to the network and thus particle growth (Dabbaghian et al., 2010).

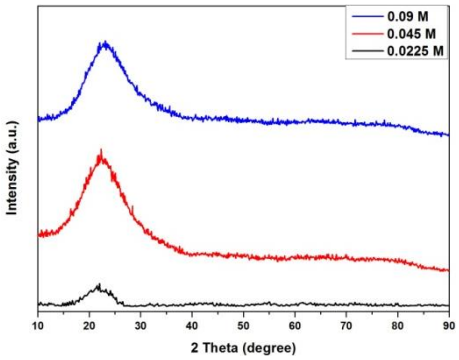


Figure 5.8 XRD results of SiO_2 nanoparticles

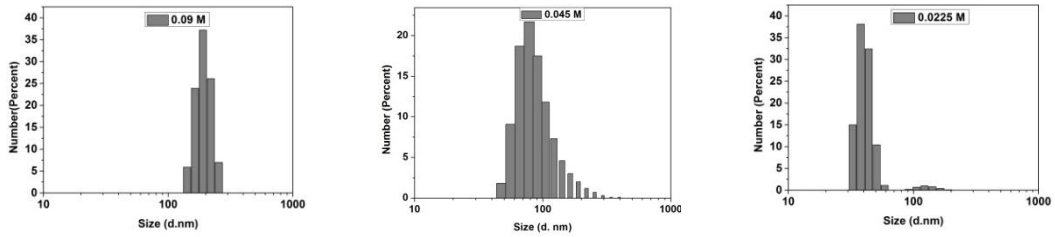


Figure 5.9 Particle size distribution chart of SiO_2 nanoparticles were synthesized using 0.09, 0045 and 0.0225 molarities

Table 5.3 Particle size values of SiO_2 nanoparticles were synthesized using different molarities

Molarite (M)	Particle size (nm)
0.09	193.5
0.045	~95
0.0225	~40.66

5.4 Characterization of Electrodeposited Pure Nickel and Nickel Matrix Nanocomposite Coatings

The X-ray diffraction patterns of pure Ni coatings prepared at different current densities are illustrated in Figure 5.10. The X-ray diffraction pattern shows typical 2θ characteristic peaks of nickel at 44.48°, 51.83° and 76.35 corresponding to (111), (200) and (220) crystallographic planes of nickel, respectively (Nickel XRD JCPDS Ref. No. 70-1849) (Rostami et al., 2013).

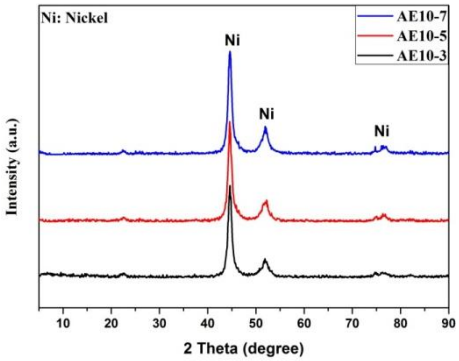


Figure 5.10 X-ray θ-2θ scans of Ni coatings at 3, 5 and 7 A dm^{-2}

5.4.1 Characterization of Electrodeposited Ni-TiO_2 Nanocomposite Coatings

The X-ray diffraction pattern of Ni–TiO_2 nanocomposite coatings electrodeposited at current density of 3, 5, 7 A dm^{-2} and nanoparticle concentrations of 1 and 3 g/l TiO_2 are shown in Fig. 5.11. The 2θ characteristic peaks of nickel at 44.48°, 51.83° and 76.35 corresponding to (111), (200) and (220) planes of the crystal lattice, respectively. However, in all electrodeposited Ni-TiO_2 coatings, the peak of TiO_2 could not be distinguished due to relatively higher intensity of nickel diffraction peaks and lower nanoparticle concentrations (Lajevardi & Shahrabi, 2010; Parida et al., 2011).

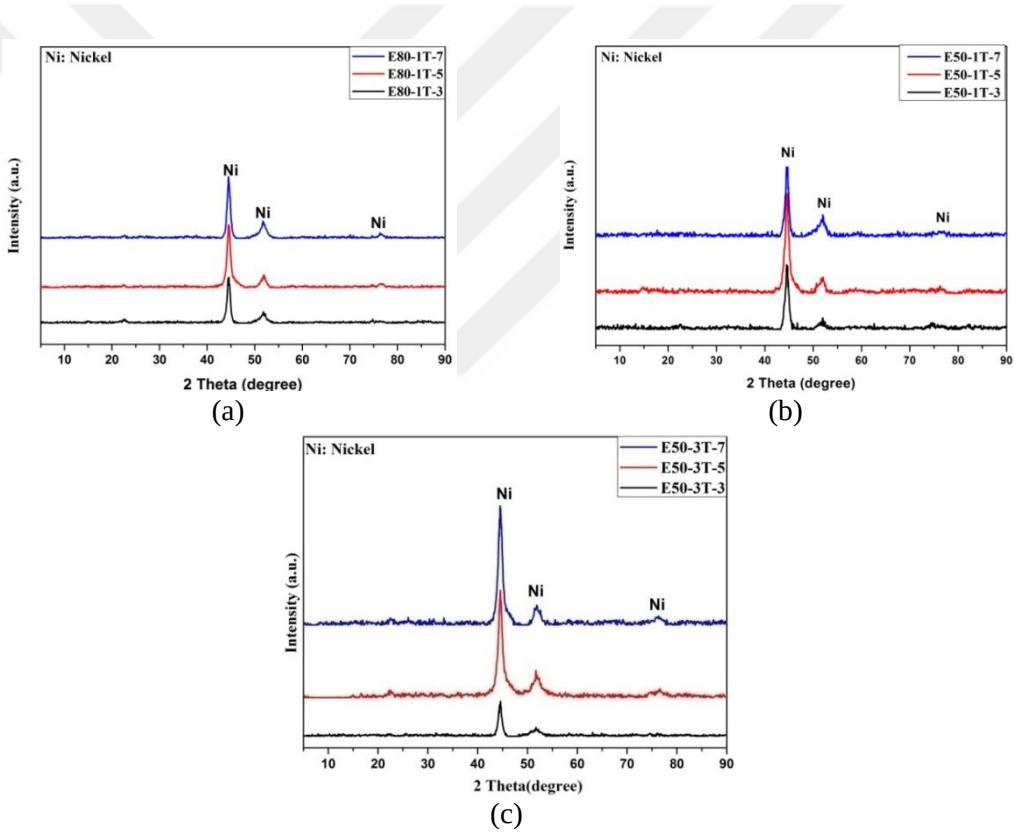


Figure 5.11 X-ray θ-2θ scans of Ni-TiO_2 nanocomposite coatings with TiO_2 nanoparticles (a) 80 nm sized and 1 g/l concentration, (b) 50 nm sized and 1 g/l concentration and (c) 50 nm sized and 3 g/l concentration electrodeposited at 3, 5 and 7 A dm^{-2} current densities.

The surface morphologies of the Ni-TiO_2 coatings analyzed by SEM are presented in Figure 5.12. Surface morphologies of Ni coatings were also given for comparison. The SEM micrographs taken for all Ni-TiO_2 samples indicate changes in morphology

depending on addition of TiO_2 nanoparticles. While pure nickel coatings have crack-free and uniform surface morphologies, TiO_2 added nickel coatings contain non-uniform structures. It was observed that non-uniform region enlarged as particle concentration increase. Similar results are observed in literature. For example Eltoum and his colleagues electrodeposited Ni-TiO_2 nanocomposite with varying titania content. And they studied the changes in microstructure and corrosion behavior of electrodeposited nickel with respect to titania addition. In their study, the addition of titania nanoparticles to the bath obviously affects the surface morphology of the coatings. They appear as light spots in the darker nickel matrix. Due to the addition of TiO_2 nanoparticles to the bath the microstructure of the nickel matrix changed from spherical to granular shape (Eltoum, Baraka, Morsi & Hassan, 2011). In another study, Baghery and his colleagues prepared Ni–TiO_2 nanocomposite coatings with various contents of TiO_2 nanoparticles by electrodeposition in a Ni plating bath. They investigate the influences of the TiO_2 nanoparticle on nanocomposite coatings. According to their experience, the pure Ni coating demonstrated a rather regular surface. The Ni–TiO_2 nanocomposite coating shows smother surface, more uniform and compact in appearance compare to that of pure Ni coating, which indicates that the codeposited TiO_2 nanoparticles were uniformly distributed in the Ni matrix of nanocomposite coating (Baghery et al., 2010). Finally, Rusu and his colleagues also focused on similar study. They prepared nanocomposites containing titanium oxide nanoparticles in a nickel matrix by means of electrodeposition process from nickel plating bath. They concluded that the surface morphology of the nickel matrix was significantly altered due to the presence of titania nanoparticles. Embedding of TiO_2 particles in the nickel matrix changes in the grain structure of the pure nickel coating. The surface of a nickel is made up of regular pyramidal crystals with a uniform grain size. The TiO_2 particles deposited with nickel radically change the structure of the metal (Rusu, Cojocaru, Magagnin, Gheorghies & Cârâc, 2010).

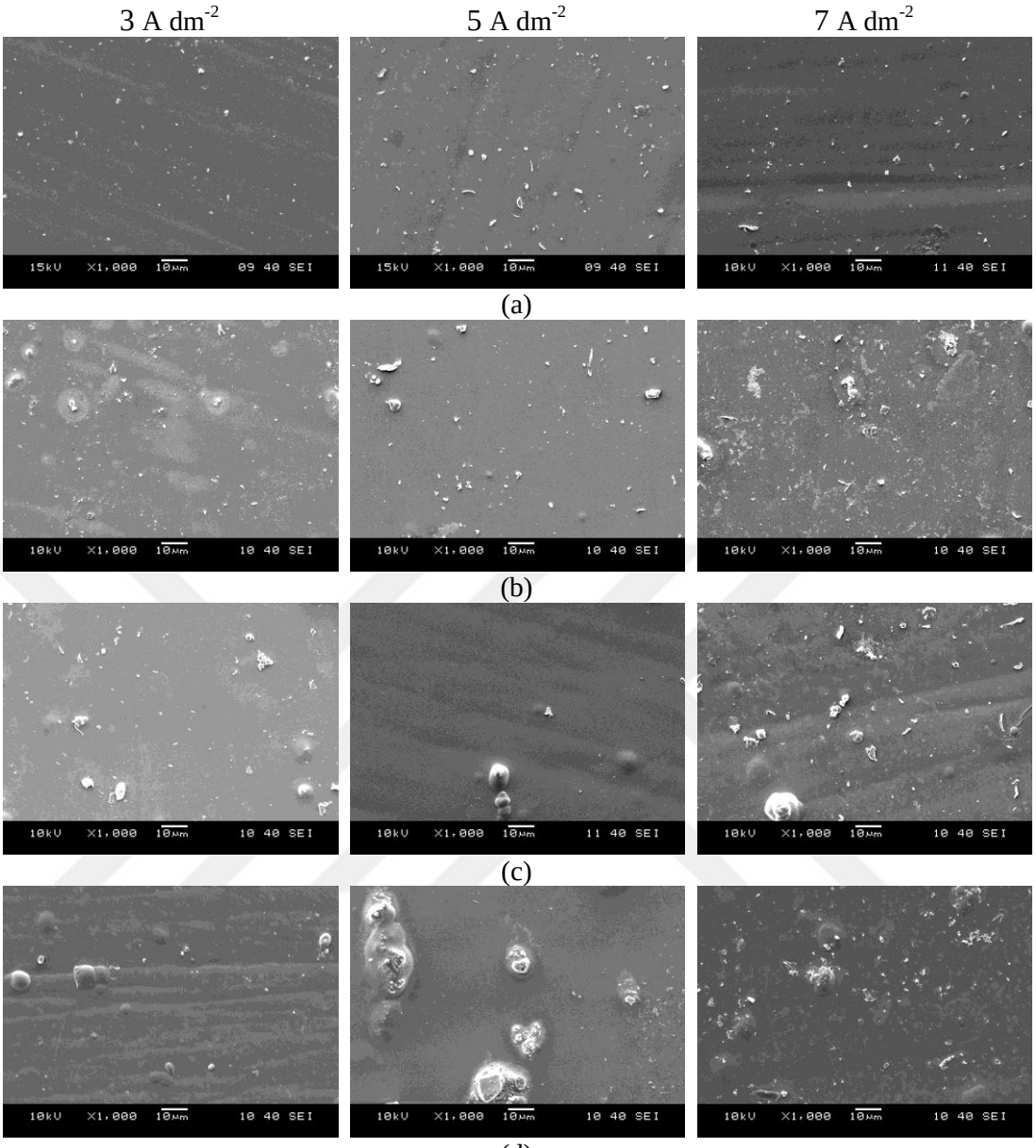


Figure 5.12 Surface morphologies of (a) pure nickel and Ni-TiO_2 nanocomposite coatings with TiO_2 nanoparticles (b) 80 nm sized and 1 g/l concentration, (c) 50 nm sized and 1 g/l concentration and (d) 50 nm sized and 3 g/l concentration electrodeposited at 3, 5 and 7 A dm^{-2} current densities.

In order to determine distribution of the TiO_2 nanoparticles in the coating structure elemental mapping was performed with EDS attached to SEM. The mapping images of E50-3T-5 coating were given to represent all of the coatings. Images of the elemental mapping for the Ni-TiO_2 nanocomposite coatings are presented in Figure 5.13 also reveal uniform distribution of the TiO_2 nanoparticles in the composite coatings under the aforesaid electrodeposition conditions.

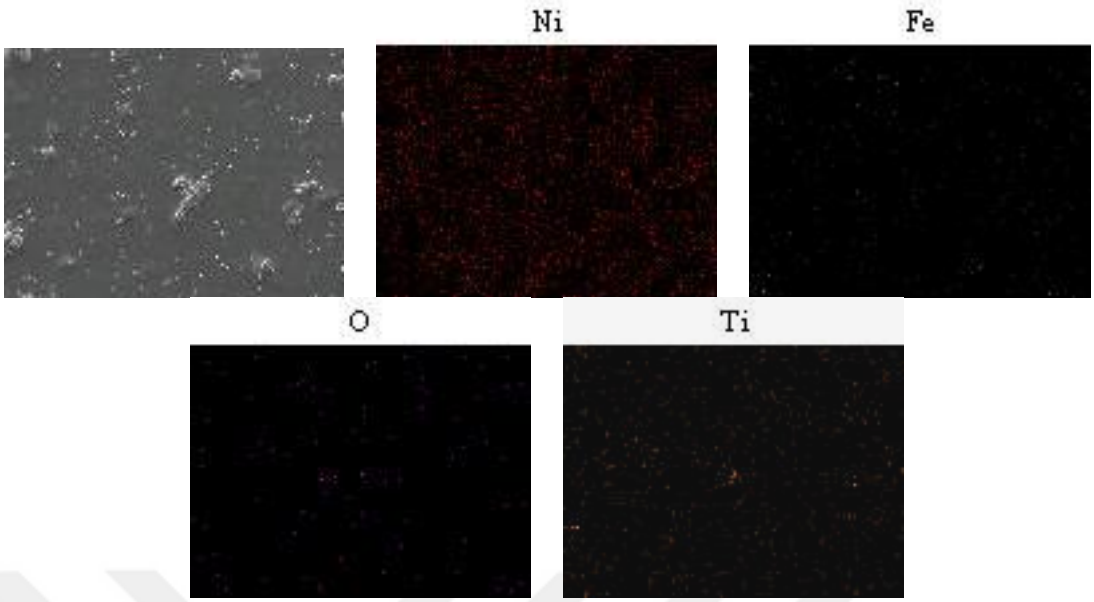
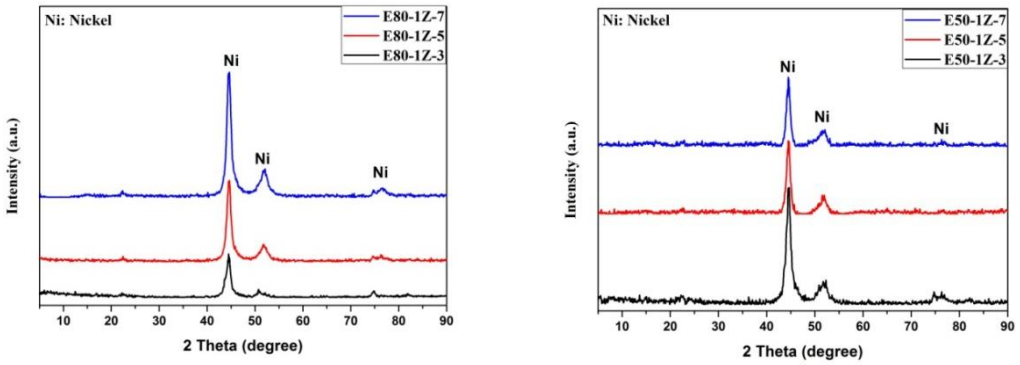


Figure 5.13 Mapping images of Ni-TiO_2 nanocomposite coatings with 50 nm sized and 3 g/l concentration TiO_2 nanoparticles

5.4.2 Characterization of Electrodeposited Ni-ZnO Nanocomposite Coatings

Figure 5.16 depicts the X-ray diffraction pattern which shows typical 2θ characteristic peaks of nickel at 44.48°, 51.83° and 76.35 corresponding to (111), (200) and (220) crystallographic planes of nickel, respectively (Nickel XRD JCPDS Ref. No. 70-1849) (Rostami et al., 2013). Further, the ZnO peaks are not discernible as well as TiO_2 peaks in Figure 5.14.



(a) (b)

Figure 5.14 X-ray θ-2θ scans of Ni-ZnO nanocomposite coatings with ZnO nanoparticles (a) 80 nm sized and 1 g/l concentration, (b) 50 nm sized and 1 g/l concentration electrodeposited at 3, 5 and 7 A dm^{-2} current densities.

Figure 5.15 compares surface morphologies of pure nickel and Ni-ZnO nanocomposite coatings electrodeposited at 3, 5 and 7 A dm^{-2} current densities with ZnO nanoparticles at 1 g/l concentration. Ni-ZnO nanocomposite coatings with 3 g/l ZnO nanoparticles concentration could not be discussed here due to the burning damage occurred at coating surface during electrodeposition process. When Figure 5.16 was examined, it is observed that both pure nickel coatings and Ni-ZnO coatings have uniform and crack-free morphologies (Wang, Zhou, Li, Zhong & Bui, 2015). It can be seen that the scratch on the pure nickel coating originate from substrate disappeared with ZnO addition.

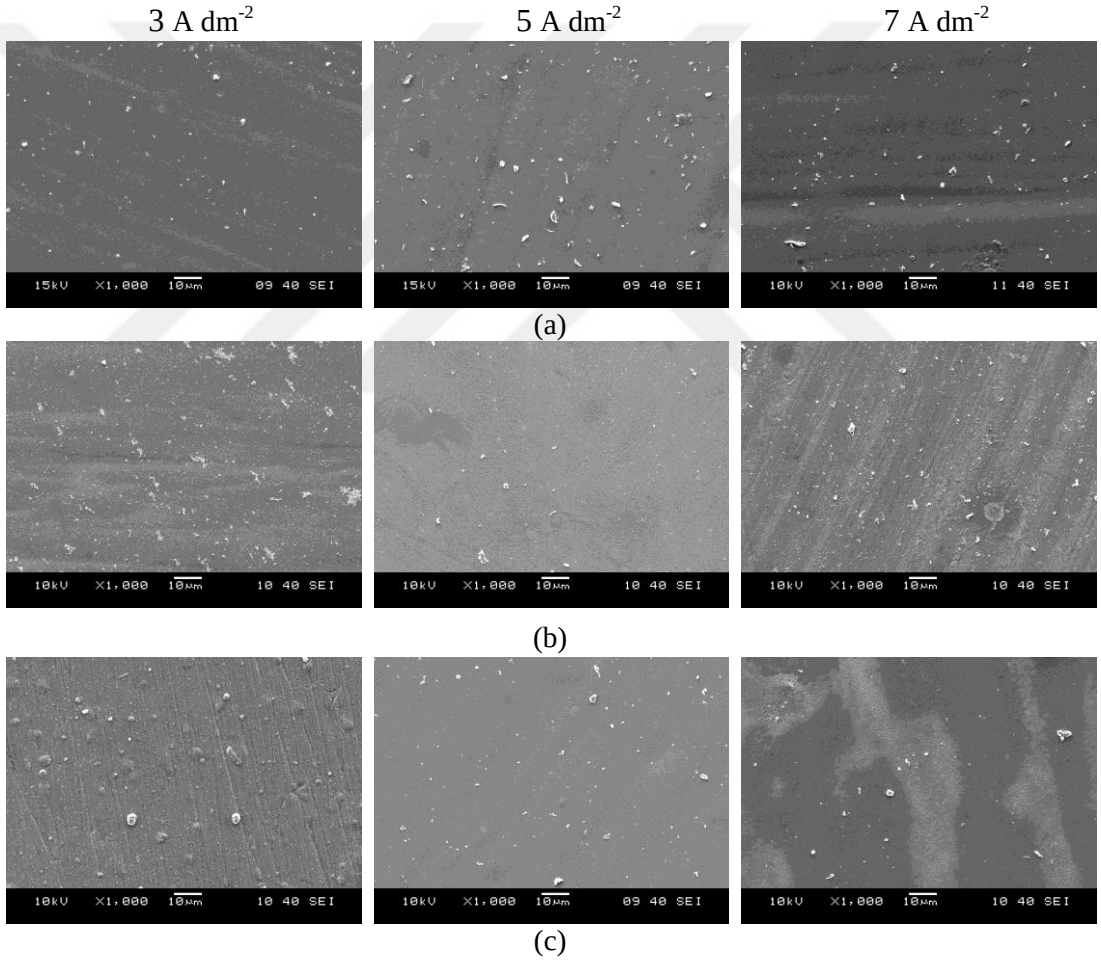


Figure 5.15 Surface morphologies of (a) pure nickel and Ni-ZnO nanocomposite coatings with ZnO nanoparticles (b) 80 nm sized and 1 g/l concentration, (c) 50 nm sized and 1 g/l concentration electrodeposited at 3, 5 and 7 A dm^{-2} current densities.

According to Elemental mapping analysis (Figure 5.16), the Zn particles were obtained on the surface of coatings. In addition the distribution of Zn particles is uniformly homogenous in all the samples.

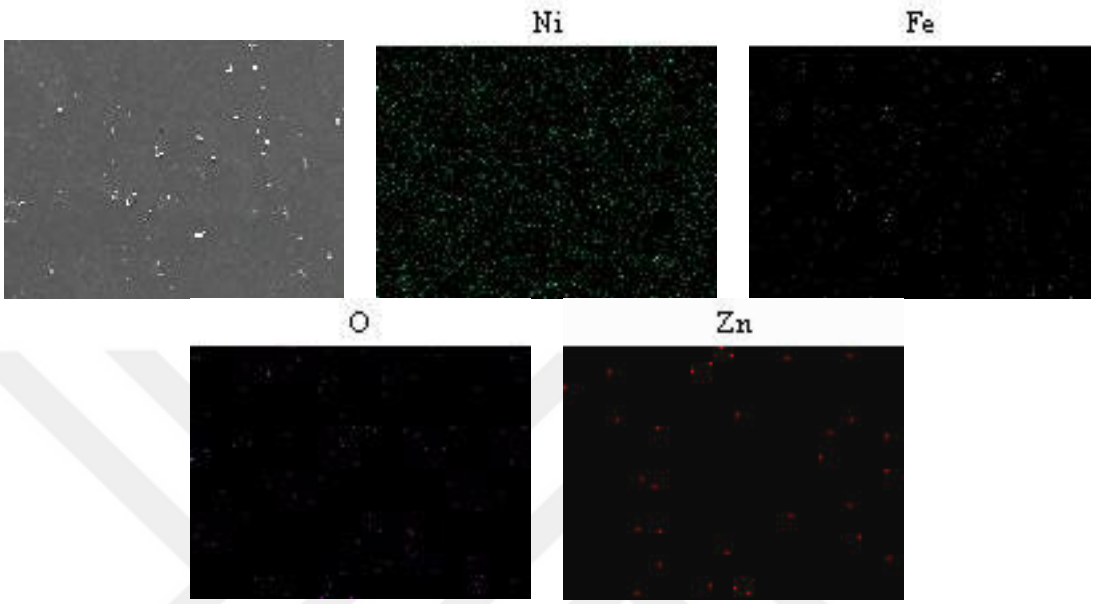
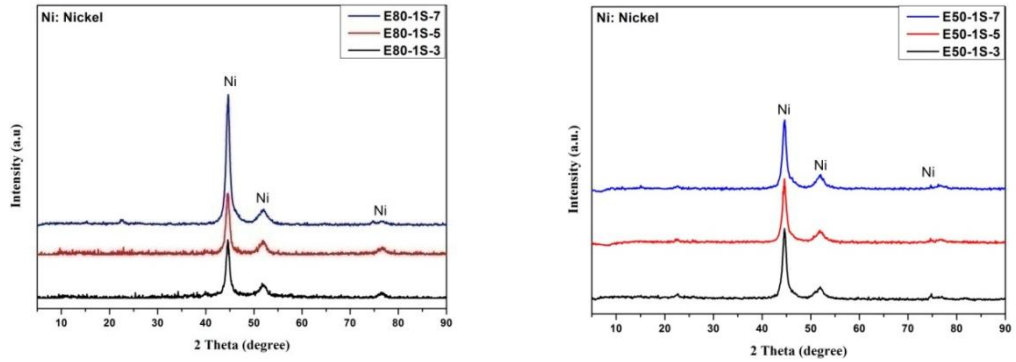


Figure 5.16 Mapping images of Ni-ZnO nanocomposite coatings with 50 nm sized and 1 g/l concentration ZnO nanoparticles

5.4.3 Characterization of Electrodeposited Ni-SiO_2 Nanocomposite Coatings

Figure 5.17 shows the X-ray diffraction pattern of Ni-SiO_2 nanocomposite coatings electrodeposited at different current densities with different particle sizes. It is seen that both coatings have typical 2θ characteristic peaks of nickel at 44.48°, 51.83° and 76.35 corresponding to (111), (200) and (220) crystallographic planes of nickel, respectively (Nickel XRD JCPDS Ref. No. 70-1849) (Rostami et al., 2013). It is seen that the X-ray diffraction pattern of the composite coating is similar to that of particle free coating because of high intensity peaks of Ni.



(a) (b)

Figure 5.17 X-ray θ-2θ scans of Ni-SiO_2 nanocomposite coatings with SiO_2 nanoparticles (a) 80 nm sized and 1 g/l concentration, (b) 50 nm sized and 1 g/l concentration and (c) 50 nm sized and 3 g/l concentration electrodeposited at 3, 5 and 7 A dm^{-2} current densities.

The SEM micrographs of Ni-SiO_2 nanocomposite coatings are shown in Figure 5.18. When these images are examined, it is obvious that both pure nickel coatings and Ni-SiO_2 coatings have crack-free morphologies. However, the micrographs of Ni-SiO_2 nanocomposite coatings are more uniform than the pure nickel coatings Wang and his colleagues obtained similar results in their study (Wang et al., 2015). Several researches have focused on Ni-SiO_2 nanocomposite coatings. For example, Yan and his friends fabricated Ni-SiO_2 nanocomposite coatings by electrodeposition on the AZ91HP magnesium alloy surface. Compared with the Ni coating, the sizes of crystal grains in the Ni-SiO_2 nanocomposite coating largely decrease due to the dimension effect of nanoparticles (Yan et al., 2011). Li and his colleagues also deposited the nano-sized SiO_2 particles in the Ni matrix by pulse electrodeposition. According to their results, the Ni-SiO_2 composite coatings are much smoother and more compact than the pure Ni coating (Li, Hou & Liang, 2016).

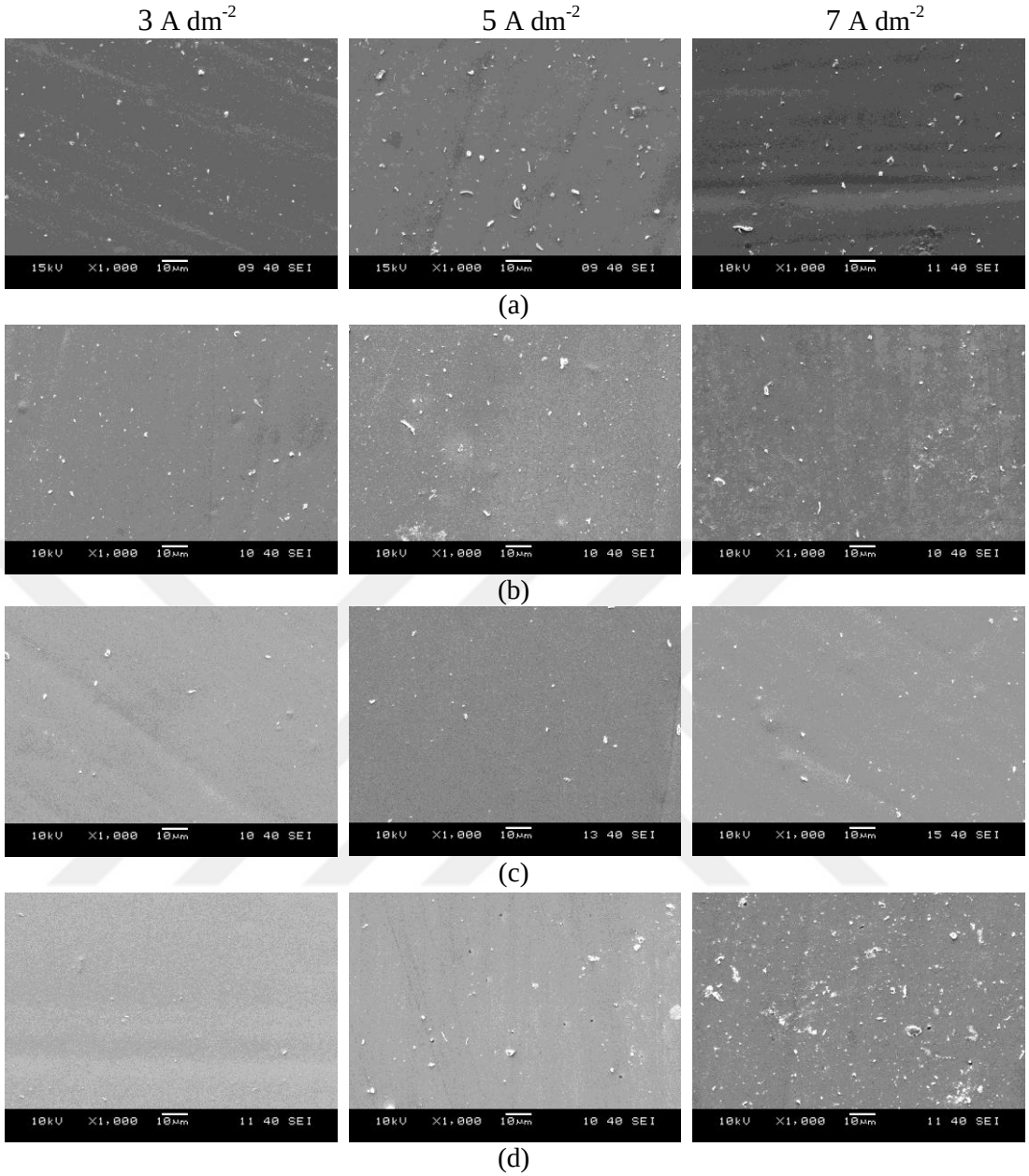


Figure 5.18 Surface morphologies of (a) pure nickel and Ni-SiO_2 nanocomposite coatings with SiO_2 nanoparticles (b) 80 nm sized and 1 g/l concentration, (c) 50 nm sized and 1 g/l concentration and (d) 50 nm sized and 3 g/l concentration electrodeposited at 3, 5 and 7 A dm^{-2} current densities.

The distribution of the SiO_2 nanoparticles are displayed by elements mapping attached to SEM. Images of the elements mapping for the Ni-SiO_2 nanocomposite coatings are presented in Figure 5.19 also reveal uniform distribution of the SiO_2 nanoparticles in the composite coatings under the aforementioned electrodeposition conditions.

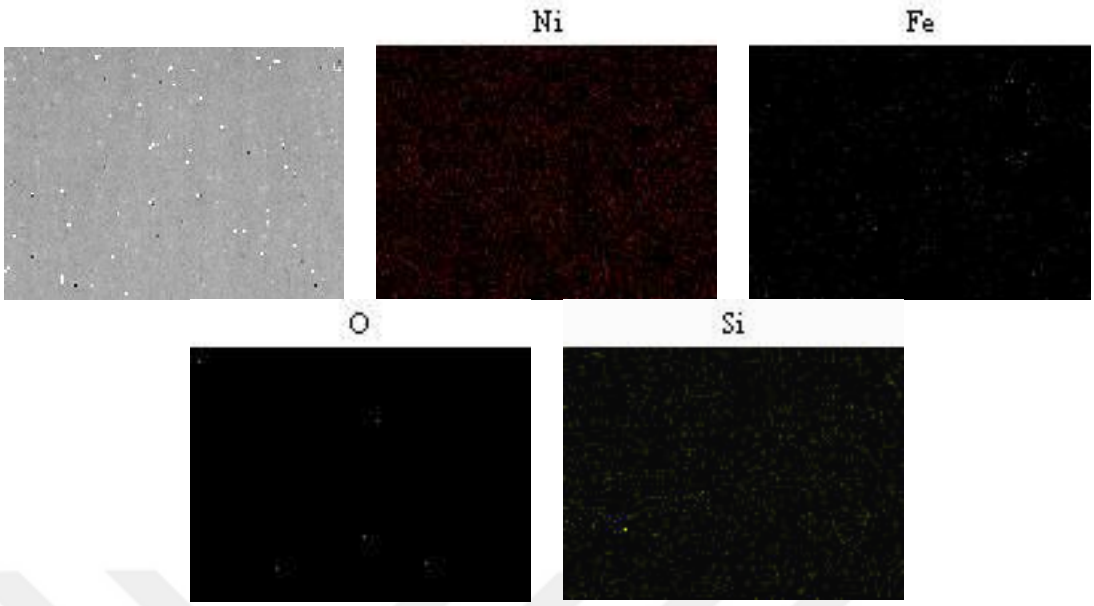


Figure 5.19 Mapping images of Ni-SiO_2 nanocomposite coatings with 50 nm sized and 3 g/l concentration SiO_2 nanoparticles

5.5 Corrosion Behavior of Electrodeposited Pure Nickel and Nickel Matrix Nanocomposite Coatings

Composite coatings that slow the rate of corrosion at a reduced cost have been extensively studied over the past several years by many researchers. Exposing films to an unfavorable environment accelerates the degradation of the film which can lead to corrosion. The rate of corrosion can be reduced using five general approaches which include the selection of materials, chemical inhibitors, changes in the environment, cathodic protection anode addition of coatings. Coatings can be produced by several different methods, and electrodeposition remains a prominent technique to produce novel materials for science and engineering applications because of many advantages as stated before (Thurber et al., 2016)

As it is mentioned in section 3.4, the corrosion performances of Ni matrix nanocomposite coatings show better corrosion performance as compared to Ni coatings. In order to improve the properties of Ni coatings, a great variety of particles such as TiO_2, Al_2O_3, CeO_2, SiC, TiC, ZrO_2, WC, ZnSe etc. have been used to enhance the performance of the metal matrix composite coatings.

Potentiodynamic polarization curves of pure Ni and Ni matrix nanocomposite coatings electrodeposited with TiO_2, ZnO and SiO_2 nanoparticles at different current densities of 3, 5 and 7 A dm^{-2} and different particle sizes in a 3.5 wt.% NaCl solution are show in Figure 5.20-5.22. Corrosion potential (E_{corr}), corrosion current density (i_{corr}), β_a, and β_c are obtained from the intersection of cathodic and anodic Tafel curve tangents and listed in Table 5.4-5.6. The corrosion rate, Corr., expressed in mm $year^{-1}$ was calculated according to the Gammry Framework software.

After stabilization of the OCPs, the potentiodynamic polarization tests were carried out for the coatings. As a result of test it was concluded that Ni-TiO_2 nanocomposite coatings show better performance than pure nickel coatings as it can be seen in Figure 5.20. Similar results are observed in literature. For example, Baghery and his colleagues prepared Ni-TiO_2 nanocomposite coatings with various contents of TiO_2 nanoparticles by electrodeposition in a Ni plating bath. They investigate the influences of the TiO_2 nanoparticle on corrosion behavior. It is obvious that with increasing of TiO_2 nanoparticle content in coating the corrosion current decreases and the corrosion potential shifts to a more positive potential. The data clearly reveals the improvement of corrosion protection by TiO_2 nanoparticles (Baghery et al., 2010). In another work, Ni-Zn-TiO_2 nanocomposite coating was fabricated using the electrodeposition process by Katamipour and his colleagues. According to their corrosion test results, all the corrosion potentials of Ni-Zn-TiO_2 nanocomposite coatings are more positive than Ni-Zn alloy coating. Otherwise, corrosion potentials shift positively with the increase of TiO_2 concentration (Katamipour, Farzam & Danaee, 2014). Finally, Ni-W-TiO_2 nanocomposite coatings have been obtained using electrodeposition method from Watts bath by Kumar and his colleagues. It was observed that corrosion current density values decreased with the incorporation of TiO_2 (Kumar, Kalaignan & Muralidharan, 2013). Moreover, in our study while E80-1T and E50-1T coatings have maximum E_{corr} and the minimum i_{corr} value at 3 A dm^{-2}, E50-3T coatings have maximum E_{corr} and the minimum i_{corr} value at 5 A dm^{-2}. E80-1T-3 and E50-3T-5 coatings which have -273 mV E_{corr} value show highest corrosion resistance (Table 5.4).

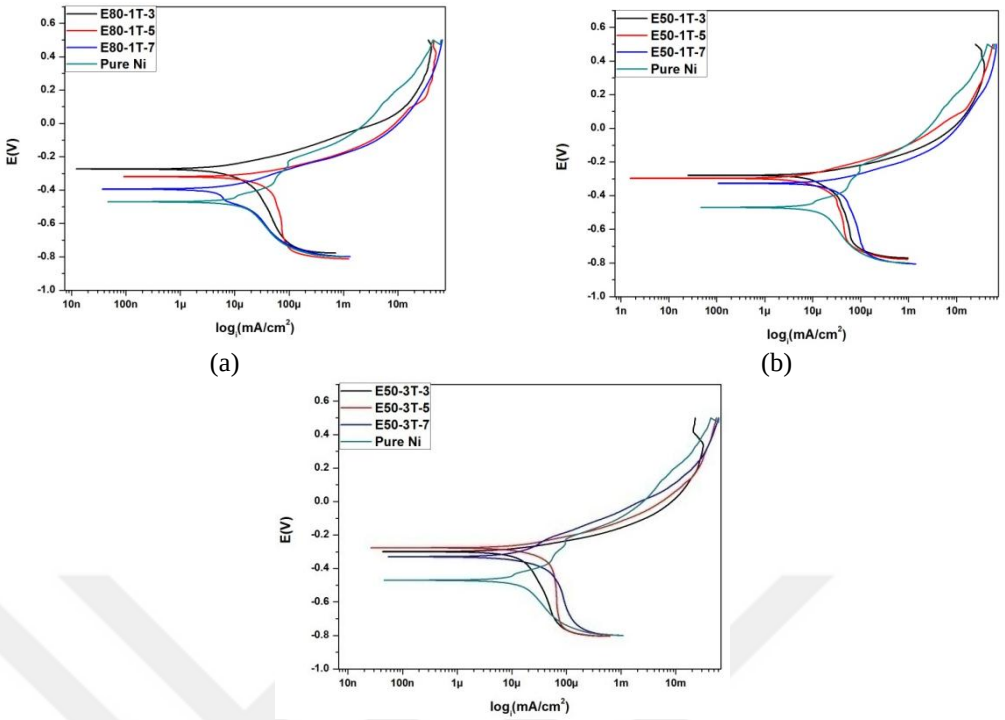


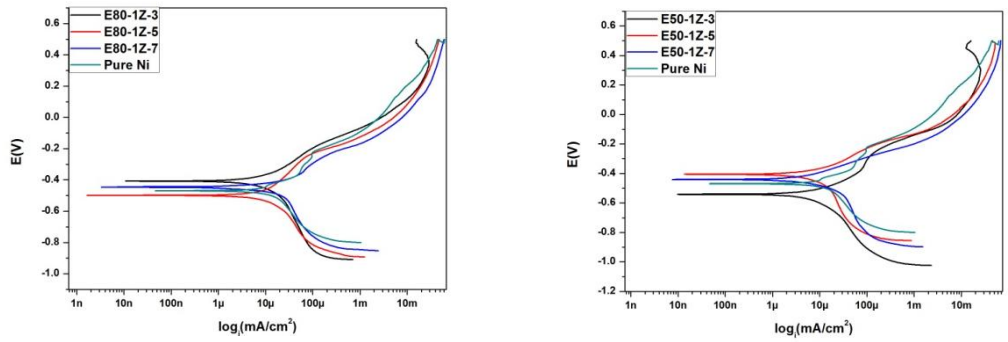
Figure 5.20 Comparative potentiodynamic diagrams of pure nickel and Ni-TiO_2 nanocomposite coatings with TiO_2 nanoparticles (a) 80 nm sized and 1 g/l concentration, (b) 50 nm sized and 1 g/l concentration and (c) 50 nm sized and 3 g/l concentration electrodeposited at 3, 5 and 7 A dm^{-2} current densities.

Table 5.4 Corrosion characteristics Ni-TiO_2 nanocomposite coatings

Coating	**E_{corr}(mV)**	**i_{corr}(mA)**	**β_a(V/decade)**	**β_c(V/decade)**	**C_{cor} rate(mpy)**
Pure Ni	-470	1.84 x 10^{-6}	0.0460	0.1118	294.3 x10^{-3}
E80-1T-3	-273	8.34 x 10^{-7}	0.0441	0.0695	133.7 x10^{-3}
E80-1T-5	-317	1.84 x 10^{-6}	0.1511	0.1764	295.4 x10^{-3}
E80-1T-7	-397	2.20 x 10^{-6}	0.0916	0.0974	353.5 x10^{-3}
E50-1T-3	-278	7.82 x 10^{-7}	0.1053	0.0869	125.3 x10^{-3}
E50-1T-5	-300	8.16 x 10^{-7}	0.1892	0.1046	130.9 x10^{-3}
E50-1T-7	-326	9.22 x 10^{-7}	0.0953	0.0873	147.9 x10^{-3}
E50-3T-3	-300	1.60 x 10^{-6}	0.1717	0.1556	256.2 x10^{-3}
E50-3T-5	-273	8.36 x 10^{-7}	0.1069	0.906	134.0 x10^{-3}
E50-3T-7	-331	3.62 x 10^{-6}	0.0737	0.0741	580.7 x10^{-3}

As it can be seen in Figures 5.21, Ni-ZnO nanocomposite coatings do not have a coherent corrosion behavior. Especially, nanocomposite coatings prepared with 50

nm ZnO nanoparticles at 3 A dm^{-2} current density and 80 nm ZnO nanoparticles at 5 A dm^{-2} exhibit corrosion potential shifts to a more negative potential which indicates deteriorated corrosion properties.



(a) (b)

Figure 5.21 Comparative potentiodynamic diagrams of pure nickel and Ni-ZnO nanocomposite coatings with ZnO nanoparticles (a) 80 nm sized and 1 g/l concentration, (b) 50 nm sized and 1 g/l concentration electrodeposited at 3, 5 and 7 A dm^{-2} current densities

Table 5.5 Corrosion characteristics Ni-ZnO nanocomposite coatings

Coating	**E_{corr}(mV)**	**i_{corr}(mA)**	**β_a(V/decade)**	**β_c(V/decade)**	**C_{cor} rate(mpy)**
Pure Ni	-470	1.84 x 10^{-6}	0.0460	0.1118	294.3 x10^{-3}
E80-1Z-3	-405	1.04 x 10^{-6}	0.0298	0.0398	166.0 x10^{-3}
E80-1Z-5	-503	5.45 x 10^{-6}	0.0608	0.0726	873.6 x10^{-3}
E80-1Z-7	-447	5.08 x 10^{-6}	0.0834	0.0999	814.9 x10^{-3}
E50-1Z-3	-538	1.05 x 10^{-5}	0.0701	0.1403	1.681
E50-1Z-5	-405	3.63 x 10^{-6}	0.1190	0.1117	582.7 x10^{-3}
E50-1Z-7	-442	4.76 x 10^{-6}	0.0626	0.0746	762.9 x10^{-3}

It can be understood that from Figure 5.22, Ni-SiO_2 nanocomposite coatings show better corrosion performance than pure nickel. Several researches have focused on Ni-SiO_2 nanocomposite coatings. For instance, Zhou and his colleagues obtained nanocomposite coatings by electrochemical codeposition of SiO_2 nano-particles with Ni-W on mild steel surface. On the contrary of our results, their electrochemical test results demonstrated that Ni-W-SiO_2 coatings exhibited a generally less protective performance compared with amorphous Ni-W coating (Wang et al., 2015). Li and his colleagues also deposited the nano-sized SiO_2 particles in the Ni matrix by pulse electrodeposition. According to their results, the Ni-SiO_2 nanocomposite coatings

exhibit much better corrosion resistance than pure Ni coating, and the corrosion resistance performance increases with increasing SiO_2 content in the composite coatings (Li et al., 2016). In our study, E80-1S and E50-1S coatings, which are obtained at 3 A dm^{-2} have maximum E_{cor} and minimum i_{cor} (Table 5.6). E_{cor} value of E50-3S coatings, which are obtained at 3 A dm^{-2} and 7 A dm^{-2} are closed to each other. These coatings have higher E_{cor} and lower i_{cor} values than coatings, obtained at 5 A dm^{-2}. Among all of the Ni-SiO_2 nanocomposite coatings, sample of E80-1S-3 which has -269 mV E_{cor} value show best corrosion performance.

Finally, when all of the coatings were examined, it could be inferred that Ni-TiO_2 nanocomposite coatings prepared with 80 nm sized nanoparticles at 3 A dm^{-2} current density has -269 mV E_{cor} value and exhibits better corrosion performance.

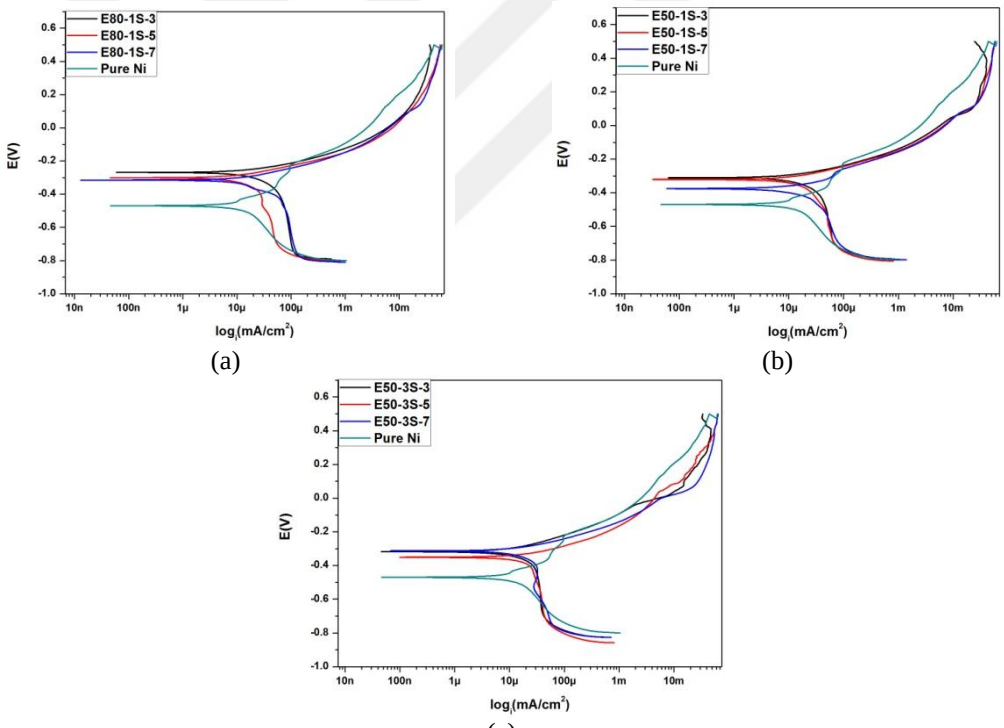


Figure 5.22 Comparative potentiodynamic diagrams of pure nickel and Ni-SiO_2 nanocomposite coatings with SiO_2 nanoparticles (a) 80 nm sized and 1 g/l concentration, (b) 50 nm sized and 1 g/l concentration and (c) 50 nm sized and 3 g/l concentration electrodeposited at 3, 5 and 7 A dm^{-2} current densities

Table 5.6 Corrosion characteristics Ni-SiO_2 nanocomposite coatings

Coating	**E_{corr}(mV)**	**i_{corr}(mA)**	**β_a(V/decade)**	**β_c(V/decade)**	**C_{cor} rate(mpy)**
Pure Ni	-470	1.84×10^{-6}	0.0460	0.1118	294.3×10^{-3}
E80-1S-3	-269	7.87×10^{-7}	0.0596	0.0829	126.3×10^{-3}
E80-1S-5	-304	1.47×10^{-6}	0.0970	0.0867	236.3×10^{-3}
E80-1S-7	-317	2.50×10^{-6}	0.0566	0.0769	400.3×10^{-3}
E50-1S-3	-310	1.46×10^{-6}	0.0892	0.0863	234.8×10^{-3}
E50-1S-5	-317	1.89×10^{-6}	0.0886	0.0949	302.4×10^{-3}
E50-1S-7	-379	3.56×10^{-6}	0.2853	0.1660	571.3×10^{-3}
E50-3S-3	-317	3.04×10^{-6}	0.1637	0.1574	487.4×10^{-3}
E50-3S-5	-353	3.52×10^{-6}	0.0403	0.0619	564.1×10^{-3}
E50-3S-7	-313	1.85×10^{-6}	0.2651	0.0796	296.7×10^{-3}

CHAPTER SIX
CONCLUSION

In this thesis, First of all TiO_2, ZnO and SiO_2 nanoparticles were synthesized by sol-gel technique. Then, Ni matrix nanocomposite coatings were prepared by electrodeposition technique on steel substrates. The effects of TiO_2, ZnO and SiO_2 nanoparticles on the microstructure, composition and the corrosion performance of Ni matrix nanocomposite coatings were investigated with different content and nano-sized particles.

Particle size distributions of nanoparticles were measured using Zeta-sizer. Crystalline structures of nanoparticles and coatings were analyzed using X-Ray Diffraction (XRD). Morphological characteristics of coatings were examined using Scanning Electron Microscopy (SEM). Additionally, corrosion properties of the coatings were studied electrochemically by potentiodynamic polarization technique in 3.5 % NaCl solution.

Findings achieved from the experimental works can be summarized as follows:

- According to XRD results, TiO_2, ZnO and SiO_2 nanoparticles are composed of anatase, zincite and amorphous phases, respectively.

- All nanoparticles were successfully synthesized in nanoscale. The average particle sizes were measured ~50 nm and ~80 nm.

- XRD results of coatings shows that nickel coatings were successfully formed on steel surface.

- According to SEM and mapping images, the coating on steel surface includes TiO_2, ZnO and SiO_2 nanoparticles.

- It is observed that Ni-TiO_2, Ni ZnO and Ni-SiO_2 nanocomposite coatings show

better corrosion performance than pure nickel coatings. However, Ni-ZnO nanocomposite coatings have lower corrosion protection as compared with Ni-TiO_2 and Ni-SiO_2 nanocomposite coatings.

REFERENCES

Ahmad, Y. H., & Mohamed, A. M. (2014). Electrodeposition of nanostructured nickel-ceramic composite coatings: A review. *International Journal of Electrochemical Sciences, 9*, 1942-1963.

Al-Bat'hi, S. A. (2015). Electrodeposition of nanostructure materials, M. Aliofkhazraei, *Nanotechnology and Nanomaterials, 6*, 954-978.

Ali, A. M., & Najmy, R. (2013). Structural, optical and photocatalytic properties of $NiO–SiO_2$ nanocomposites prepared by sol–gel technique. *Catalysis Today, 208*, 2-6.

Alias, S., Ismail, A., & Mohamad, A. (2010). Effect of ph on ZnO nanoparticle properties synthesized by sol–gel centrifugation. *Journal of Alloys and Compounds, 499* (2), 231-237.

Andrievski, R., & Glezer, A. (2001). Size effects in properties of nanomaterials. *Scripta Materialia, 44* (8), 1621-1624.

Andrievski, R. A. (2001). Nano-metals. Films as nanostructured materials with characteristic mechanical properties. *Materials Transactions, 42* (8), 1471-1473.

Avril, L., Bourgeois, S., de Lucas, M. M., Domenichini, B., Simon, P., Addou, F., et al. (2015). Thermal stability of $Au–TiO_2$ nanocomposite films prepared by direct liquid injection cvd. *Vacuum, 122*, 314-320.

Bagheri, S., Shameli, K., & Abd Hamid, S. B. (2012). Synthesis and characterization of anatase titanium dioxide nanoparticles using egg white solution via sol-gel method. *Journal of Chemistry, 2013*.

Baghery, P., Farzam, M., Mousavi, A. ,& Hosseini, M. (2010). Ni–TiO_2 nanocomposite coating with high resistance to corrosion and wear. *Surface and Coatings Technology, 204* (23), 3804-3810.

Bakshi, S., Lahiri, D., & Agarwal, A. (2010). Carbon nanotube reinforced metal matrix composites-a review. *International Materials Reviews, 55* (1), 41-64.

Baron, A., Szewieczek, D., & Nowosielski, R. (2007). Selected manufacturing techniques of nanomaterials. *Journal of Achievements in Materials and Manufacturing Engineering, 20* (1-2), 83-86.

Beltowska-Lehman, E., Indyka, P., Bigos, A., Szczerba, M., & Kot, M. (2016). Effect of hydrodynamic conditions of electrodeposition process on microstructure and functional properties of Ni-W/ZrO_2 nanocomposites. *Journal of Electroanalytical Chemistry, 775*, 27-36.

Bevins, C. L., & Zasloff, M. (1990). Peptides from frog skin. *Annual Review of Biochemistry, 59* (1), 395-414.

Borkar, T., & Harimkar, S. P. (2011). Effect of electrodeposition conditions and reinforcement content on microstructure and tribological properties of nickel composite coatings. *Surface and Coatings Technology, 205* (17), 4124-4134.

Branda, F. (2011). *The sol-gel route to nanocomposites*: INTECH Open Access Publisher.

Callister, W. D., & Rethwisch, D. G. (2007). *Materials science and engineering: An introduction*. New York: Wiley.

Callister, W. D., & Rethwisch, D. G. (2012). *Fundamentals of materials science and engineering: An integrated approach*: John Wiley & Sons.

Camargo, P. H. C., Satyanarayana, K. G., & Wypych, F. (2009). Nanocomposites: Synthesis, structure, properties and new application opportunities. *Materials Research, 12* (1), 1-39.

Cantor, B., Allen, C., Dunin-Burkowski, R., Green, M., Hutchinson, J., O'Reilly, K., et al., (2001). Applications of nanocomposites. *Scripta Materialia, 44* (8), 2055-2059.

Charitidis, C. A., Georgiou, P., Koklioti, M. A., Trompeta, A.-F., & Markakis, V. (2014). Manufacturing nanomaterials: From research to industry. *Manufacturing Review, 1*, 11.

Chou, M.-C., Ger, M.-D., Ke, S.-T., Huang, Y.-R., & Wu, S.-T. (2005). The Ni-P-SiC composite produced by electro-codeposition. *Materials Chemistry and Physics, 92* (1), 146-151.

Collins, A. M. (2012). Chapter 4: Chemical techniques. *Nanotechnology cookbook*, 35-204.

Dabbaghian, M., Babalou, A., Hadi, P., & Jannatdoust, E. (2010). A parametric study of the synthesis of silica nanoparticles via sol-gel precipitation method. *International Journal of Nanoscience and Nanotechnology, 6* (2), 104-113.

Dennis, J. K., & Such, T. E. (1993). *Nickel and chromium plating*: Elsevier.

Di Bari, G. A. (2000). Electrodeposition of nickel. *Modern Electroplating, 5*, 79-114.

Doeuff, S., Henry, M., Sanchez, C., & Livage, J. (1987). Hydrolysis of titanium alkoxides: Modification of the molecular precursor by acetic acid. *Journal of Non-Crystalline Solids, 89* (1), 206-216.

Donald, W. B. (1994). Surface engineering. *Electroless Nickel Plating*, 5, 290-305.

Dubpernell, G. (1959). *The story of nickel plating*: M., & T. Chemicals, Incorporated.

Eltoum, M. A., Baraka, A., Morsi, M., & Hassan, E. A. (2011). Electrodeposition and characterization of nickel–titania nanocomposite coatings from gluconate baths. *International Journal Of Multidisciplinary Sciences And Engineering, 2* (4).

Feddes, B., González, P., Serra, J., Pou, J., Chiussi, S., Wolke, J. G., et al., (2009). Characterization of thin calcium phosphate coating. In *Thin Calcium Phosphate Coatings for Medical Implants* (25-66): Springer.

Fiiipponi, L., & Sutherland, D. (2012). *Nanotechnologies: Principles, applications, implications and hands-on activities: A compendium for educators*: European Union, Directorate General for Research and Innovation.

Ger, M.-D. (2004). Electrochemical deposition of nickel/SiC composites in the presence of surfactants. *Materials Chemistry and Physics, 87* (1), 67-74.

Gogotsi, Y. (2006). *Nanomaterials handbook*: CRC Press.

Gorji, B., Ghasri, M. A., Fazaeli, R., & Niksirat, N. (2012). Synthesis and characterizations of silica nanoparticles by a new sol-gel method. *Journal of Applied Chemical Research, 6* (3), 22-26.

Guo, C., Zuo, Y., Zhao, X., Zhao, J., & Xiong, J. (2008). The effects of electrodeposition current density on properties of Ni–CNTs composite coatings. *Surface and Coatings Technology, 202* (14), 3246-3250.

Gusev, A. I. (1998). Effects of the nanocrystalline state in solids. *Physics-Uspekhi, 41* (1), 49-76.

Holister, P., Weener, J., Vas, C., & Harper, T. (2003). *Nanoparticles; technology white papers*, Cientifica.

Holubar, P., Jilek, M., & Sima, M. (2000). Present and possible future applications of superhard nanocomposite coatings. *Surface and Coatings Technology, 133*, 145-151.

Horikoshi, S., & Serpone, N. (2013). Introduction to nanoparticles. *Microwaves in Nanoparticle Synthesis: Fundamentals and Applications*, 1-24.

Hou, K., Ger, M., Wang, L., & Ke, S. (2002). The wear behaviour of electro-codeposited Ni–SiC composites. *Wear, 253* (9), 994-1003.

Kalska-Szostko, B. (2012). *Electrochemical methods in nanomaterials preparation*: INTECH Open Access Publisher.

Karbasi, M., Yazdian, N., & Vahidian, A. (2012). Development of electro-co-deposited Ni–TiC nano-particle reinforced nanocomposite coatings. *Surface and Coatings Technology, 207*, 587-593.

Katamipour, A., Farzam, M., & Danaee, I. (2014). Effects of sonication on anticorrosive and mechanical properties of electrodeposited Ni–Zn–TiO_2 nanocomposite coatings. *Surface and Coatings Technology, 254*, 358-363.

Kentepozidou, A., Kiparissides, C., Kotzia, F., Kollia, C., & Spyrellis, N. (1996). Nickel/microcapsules composite electrocoatings; the synthesis of water-containing microcapsules and preparation of the coatings. *Journal of Materials Science, 31* (5), 1175-1181.

Kim, S. K., & Yoo, H. J. (1998). Formation of bilayer Ni–SiC composite coatings by electrodeposition. *Surface and Coatings Technology, 108*, 564-569.

Kruis, F. E., Fissan, H., & Peled, A. (1998). Synthesis of nanoparticles in the gas phase for electronic, optical and magnetic applications—a review. *Journal of Aerosol Science, 29* (5), 511-535.

Kumar, K. A., Kalaignan, G. P., & Muralidharan, V. (2013). Direct and pulse current electrodeposition of Ni–W–TiO_2 nanocomposite coatings. *Ceramics International, 39* (3), 2827-2834.

Lajevardi, S., & Shahrabi, T. (2010). Effects of pulse electrodeposition parameters on the properties of Ni–TiO_2 nanocomposite coatings. *Applied Surface Science, 256* (22), 6775-6781.

Li, R., Hou, Y., & Liang, J. (2016). Electro-codeposition of Ni-SiO_2 nanocomposite coatings from deep eutectic solvent with improved corrosion resistance. *Applied Surface Science, 367*, 449-458.

Macwan, D., Dave, P. N., & Chaturvedi, S. (2011). A review on nano-TiO_2 sol–gel type syntheses and its applications. *Journal of Materials Science, 46* (11), 3669-3686.

Mahshid, S., Ghamsari, M. S., Askari, M., Afshar, N., & Lahuti, S. (2006). Synthesis of TiO_2 nanoparticles by hydrolysis and peptization of titanium isopropoxide solution. *Semiconductor Physics, Quantum Electronics & Optoelectronics, 9* (2), 65-68.

Manias, E. (2007). Nanocomposites: Stiffer by design. *Nature Materials, 6* (1), 9-11.

Maya, L., Allen, W., Glover, A., & Mabon, J. (1995). Gold nanocomposites. *Journal of Vacuum Science & Technology B, 13* (2), 361-365.

Mazaleyrat, F., & Varga, L. (2000). Ferromagnetic nanocomposites. *Journal of Magnetism and Magnetic Materials, 215*, 253-259.

Metal plating processes and methods of measuring surface hardness and thickness of coatings. (n.d.). Retrieved August 1, 2016, from http://www.balseal.com/sites/default/files/tr105_020707140651.pdf

Moncada, E., Quijada, R., & Retuert, J. (2007). Nanoparticles prepared by the sol–gel method and their use in the formation of nanocomposites with polypropylene. *Nanotechnology, 18* (33), 335606.

Musić, S., Filipović-Vinceković, N., & Sekovanić, L. (2011). Precipitation of amorphous SiO_2 particles and their properties. *Brazilian Journal of Chemical Engineering, 28* (1), 89-94.

Musil, J. (2000). Hard and superhard nanocomposite coatings. *Surface and Coatings Technology, 125* (1), 322-330.

Niederberger, M., & Pinna, N. (2009). Aqueous and nonaqueous sol-gel chemistry. *Metal Oxide Nanoparticles in Organic Solvents: Synthesis, Formation, Assembly and Application*, 7-18.

Niu, Z.-X., Cao, F.-H., Wei, W., Zhang, Z., Zhang, J.-Q., & Cao, C.-N. (2007). Electrodeposition of Ni-SiC nanocomposite film. *Transactions of Nonferrous Metals Society of China, 17* (1), 9-15.

Öchsner, A. (2009). *Nanocomposite coatings and nanocomposite materials:*, Trans Tech Publications.

Parida, G., Chaira, D., Chopkar, M., & Basu, A. (2011). Synthesis and characterization of Ni-TiO_2 composite coatings by electro-co-deposition. *Surface and Coatings Technology, 205* (21), 4871-4879.

Pierre, A. C. (2013). *Introduction to sol-gel processing*: Springer Science & Business Media.

Provenzano, V., & Holtz, R. (1995). Nanocomposites for high temperature applications. *Materials Science and Engineering: A, 204* (1), 125-134.

Qiao, S., Liu, J., & Lu, G. (2011). Synthetic chemistry of nanomaterials. *Modern Inorganic Synthetic Chemistry, 6*, 479-506

Rahman, I. A., & Padavettan, V. (2012). Synthesis of silica nanoparticles by sol-gel: Size-dependent properties, surface modification, and applications in silica-polymer nanocomposites-a review. *Journal of Nanomaterials, 2012*, 8.

Ranganathan, K., Morais, A., Nongwe, I., Longo, C., Nogueira, A. F., & Coville, N. J. (2015). Study of photoelectrochemical water splitting using composite films based on TiO_2 nanoparticles and nitrogen or boron doped hollow carbon spheres as photoanodes. *Journal of Molecular Catalysis A: Chemical*, *422*, 165-174.

Rani, S., Suri, P., Shishodia, P., & Mehra, R. (2008). Synthesis of nanocrystalline zno powder via sol–gel route for dye-sensitized solar cells. *Solar Energy Materials and Solar Cells, 92* (12), 1639-1645.

Rao, K. S., El-Hami, K., Kodaki, T., Matsushige, K., & Makino, K. (2005). A novel method for synthesis of silica nanoparticles. *Journal of Colloid and Interface Science, 289* (1), 125-131.

Rashidi, A., & Amadeh, A. (2009). The effect of saccharin addition and bath temperature on the grain size of nanocrystalline nickel coatings. *Surface and Coatings Technology*, *204* (3), 353-358.

Rose, I., & Whittington, C. (2002). *Nickel plating handbook*. OM Group, Espoo, Finland.

Rostami, M., Fahami, A., Nasiri-Tabrizi, B., Ebrahimi-Kahrizsangi, R., & Saatchi, A. (2013). Characterization of electrodeposited Ni–SiC–Cg nanocomposite coating. *Applied Surface Science, 265*, 369-374.

Rusu, D., Cojocaru, P., Magagnin, L., Gheorghies, C., & Cârâc, G. (2010). Study of Ni-TiO_2 nanocomposite coating prepared by electrochemical deposition. *Journal of Optoelectronics and Advanced Materials, 12* (12), 2419-2422.

Sadiku-Agboola, O., Sadiku, E., Ojo, O., Akanji, O., & Biotidara, O. (2011). Influence of operation parameters on metal deposition in bright nickel-plating process. *Portugaliae Electrochimica Acta, 29* (2), 91-100.

Sadreddini, S., & Afshar, A. (2014). Corrosion resistance enhancement of Ni-P-nano SiO_2 composite coatings on aluminum. *Applied Surface Science, 303*, 125-130.

Saidin, N. U., Ying, K., & Khuan, N. (2011). *Electrodeposition: Principles, applications and methods*. Retrieved May 5, 2016, from http://www.iaea.org/inis/collection/NCLCollectionStore/_Public/44/122/44122714.pdf

Sangchay, W., Sikong, L., & Kooptarnond, K. (2012). Comparison of photocatalytic reaction of commercial p25 and synthetic TiO_2-AgCl nanoparticles. *Procedia Engineering, 32*, 590-596.

Schodek, D. L., Ferreira, P., & Ashby, M. F. (2009). *Nanomaterials, nanotechnologies and design: An introduction for engineers and architects*: Butterworth-Heinemann.

Sharmila Devi, R., Venckatesh, R., & Sivaraj, R. (2014). Synthesis of titanium dioxide nanoparticles by sol–gel technique. *International Journal of Innovative Research in Science Engineering and Technology*, *3* (8), 15206-15211.

Shibli, S., Jabeera, B., & Anupama, R. (2006). Development of ZnO incorporated composite Ni–ZnO–P alloy coating. *Surface and Coatings Technology, 200* (12), 3903-3906.

Shirke, B., Korake, P., Hankare, P., Bamane, S., & Garadkar, K. (2011). Synthesis and characterization of pure anatase TiO_2 nanoparticles. *Journal of Materials Science: Materials in Electronics, 22* (7), 821-824.

Singh, N. (2012). Effect of ageing in structural properties of ZnO nanoparticles with ph variation for application in solar cells. *The Open Renewable Energy Journal, 5*, 15-18.

Spanou, S., Pavlatou, E., & Spyrellis, N. (2009). Ni/nano-TiO_2 composite electrodeposits: Textural and structural modifications. *Electrochimica Acta, 54* (9), 2547-2555.

Stroumbouli, M., Gyftou, P., Pavlatou, E., & Spyrellis, N. (2005). Codeposition of ultrafine WC particles in ni matrix composite electrocoatings. *Surface and Coatings Technology, 195* (2), 325-332.

Swihart, M. T. (2003). Vapor-phase synthesis of nanoparticles. *Current Opinion in Colloid and Interface Science, 8* (1), 127-133.

Thiemig, D., & Bund, A. (2008). Characterization of electrodeposited Ni–TiO_2 nanocomposite coatings. *Surface and Coatings Technology, 202* (13), 2976-2984.

Thurber, C. R., Ahmad, Y. H., Sanders, S. F., Al-Shenawa, A., D'Souza, N., Mohamed, A. M. et al., (2016). Electrodeposition of 70-30 Cu–Ni nanocomposite coatings for enhanced mechanical and corrosion properties. *Current Applied Physics, 16* (3), 387-396.

Tseng, T. K., Lin, Y. S., Chen, Y. J., & Chu, H. (2010). A review of photocatalysts prepared by sol-gel method for vocs removal. *International Journal of Molecular Sciences, 11* (6), 2336-2361.

Vaz, F., & Rebouta, L. (2001). Superhard nanocomposite Ti-Si-N coatings *Materials science forum* (Vol. 383, 143-150): Trans Tech Publications.

Veprek, S., & Argon, A. S. (2001). Mechanical properties of superhard nanocomposites. *Surface and Coatings Technology, 146*, 175-182.

Vepřek, S., & Reiprich, S. (1995). A concept for the design of novel superhard coatings. *Thin Solid Films, 268* (1), 64-71.

Wang, Q. J., & Chung, Y.-W. (2013). Tribology. In *Encyclopedia of Tribology* (3816-3818): Springer.

Wang, Y., Zhou, Q., Li, K., Zhong, Q., & Bui, Q. B. (2015). Preparation of Ni–W–SiO_2 nanocomposite coating and evaluation of its hardness and corrosion resistance. *Ceramics International, 41* (1), 79-84.

Willems, V. D. W. (2005). *Roadmap report on nanoparticles*. W&W Espana sl, Barcelona, Spain, 1-57.

Yan, L., Yu, S.-R., Liu, J.-D., Han, Z.-W., & Yuan, D.-S. (2011). Microstructure and wear resistance of electrodeposited Ni-SiO_2 nano-composite coatings on AZ91HP magnesium alloy substrate. *Transactions of Nonferrous Metals Society of China, 21*, 483-488.

Zhang, S., Sun, D., Fu, Y., & Du, H. (2003). Recent advances of superhard nanocomposite coatings: A review. *Surface and Coatings Technology, 167* (2), 113-119.